

**ENHANCED OIL RECOVERY (EOR) BY USING EM TRANSMITTER
AND COBALT FERRITE MAGNETIC NANOPARTICLES**

By

NOORASIKIN BINTI MOHD YUSOF

Dissertation Report Submitted to the
Electrical & Electronics Engineering Programme
in Partial Fulfillment of the Requirements
for the Degree
Bachelor of Engineering (Hons)
(Electrical & Electronics Engineering)

MAY 2011

Universiti Teknologi PETRONAS
Bandar Seri Iskandar
31750 Tronoh
Perak Darul Ridzuan.

CERTIFICATION OF APPROVAL

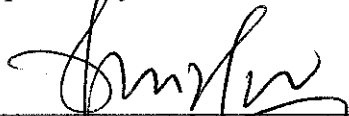
ENHANCED OIL RECOVERY (EOR) BY USING EM TRANSMITTER AND COBALT FERRITE MAGNETIC NANOPARTICLES

by

Noorasikin Binti Mohd Yusof

Dissertation report submitted to the
Electrical & Electronics Engineering Programme
Universiti Teknologi PETRONAS
in partial fulfilment of the requirement for the
Bachelor of Engineering (Hons)
(Electrical & Electronics Engineering)

Approved by:



PROF. DR. NOORHANA YAHYA

Professor Dr. Noorhana Yahya
Project Supervisor

Dean

Faculty of Science & Information Technology

Universiti Teknologi PETRONAS

TRONOH, PERAK

May 2011

CERTIFICATION OF ORIGINALITY

This is to certify that I am responsible for the work submitted in this project, that the original work is my own except as specified in the references and acknowledgements, and that the original work contained herein have not been undertaken or done by unspecified sources or persons.



NOORASIKIN BINTI MOHD YUSOF

ABSTRACT

It is practically impossible to extract crude oil from a reservoir completely. There are four common methods of Enhanced Oil Recovery (EOR) used in the industry which are thermal recovery; chemical injection; gas injection; and ultrasonic approach. The idea of this project is to improve the existing Enhanced Oil Recovery (EOR) methods, where Electromagnetic (EM) transmission system is going to be used as a safer, cheaper, reusable and simple tool that can help to increase the production of crude oil in industry. This project deals with synthesis of cobalt ferrite, CoFe_2O_4 , nanoparticles via sol- gel method. Crystallography, chemical composition and morphology of the samples were analyzed by using X-Ray Diffractometer (XRD), Field Emission Scanning Electron Microscope (FESEM) and Energy Dispersive X-Ray (EDX). By using XRD result, the crystallite size of the mixture annealed at 800°C is 5.1171nm , calculated by using Scherer's equation. FESEM result shows the grain size is in range 26nm - 36nm . From EDX result, Cobalt ferrite sample anneal at 800°C is chosen because it has lower standard deviation of Co, Fe, and O which are 24%, 7.18% and 9.59% respectively. The initial permeability of cobalt ferrite powder was found to increase and relative loss factor decreased at high frequency. Hence, cobalt ferrite prepared at 800°C exhibit good crystal structure, fine grain size, and good magnetic properties. Cobalt ferrite nanofluid was prepared by dispersing 5g cobalt ferrite nanopowder and 5g Sodium Dodecyl Sulphate (SDS) in 500ml deionized water and ultrasonicated for 2 hours, which then injected into a packed glass bead column (reservoir model). Electromagnetic (EM) wave transmission system is used with nanofluid injection to the reservoir model that helps to reduce the interfacial tension of the oil and water. This is because the nanofluid (cobalt ferrite) plays as electromagnetic wave absorption material, where the molecules start to vibrate, moving apart more frequently and thus disturb the compatibility at oil-water interfaces. Hence, the mobility of oil will improve. After conducting

experiment with transmitter with nanofluid injection, about 31.58% oil is recovered from residual oil in place (ROIP).

ACKNOWLEDGEMENT

I would like to take this opportunity to express my gratitude to those who had assisted me in completing Final Year Project (FYP). First of all, I would like to express my appreciation to my supervisors, Professor Dr. Noorhana Binti Yahya, for all her guidance, advices and concern in this project. I also would like to extend my appreciation to the postgraduate students especially Noor Rasyada Ahmad Latiff and Poppy Puspitasari for their acceptance, co-operation and willingness to share the knowledge and experience with me on handling this project. To teach a person with little knowledge and experience on the project really needs a lot of patients and knowledge. Thanks again to them. My appreciation also goes to my entire colleague and the lab technician for their help and concern during the FYP periods. Finally, I would like to express gratitude to everybody who helped me directly and indirectly throughout this Final Year Project.

TABLE OF CONTENTS

ABSTRACT	iv
LIST OF FIGURES	ix
LIST OF TABLES	xii
CHAPTER 1 INTRODUCTION	1
1.1 Background of study	1
1.2 Problem statement.....	4
1.3 Objectives	4
1.4 Scope of study	4
1.5 Feasibility of the project	5
CHAPTER 2 LITERATURE REVIEW	6
2.1 Magnetic nanoparticles	6
2.2 Sol gel technique for preparation of the magnetic nanoparticles	8
2.3 Electromagnetic wave for EOR	9
2.4 Electromagnetic transmitter	13
2.4.1 Radiation pattern	12
2.4.2 Directivity	13
2.4.3 Gain.....	14
2.4.4 Efficiency.....	14
2.5 Magnetic saturation.....	15
2.6 Permeability	16
2.7 Interfacial tension.....	17
CHAPTER 3 METHODOLOGY	19
3.1 Procedure identification	19
3.2 Tools required	21

CHAPTER 4 RESULT AND DISCUSSIONS	29
4.1 Synthesis of Coabl ^t Ferrite.....	29
4.1.1 <i>Experiment procedure</i>	29
4.1.2 <i>Calculation of Cobalt Ferrite using sol gel method</i>	30
4.2 Characterization of Cobalt Ferrite	36
4.2.1 <i>X-Ray Diffraction (XRD) Results</i>	36
4.2.2 <i>FESEM Results</i>	40
4.2.3 <i>EDX Results</i>	42
4.2.4 <i>Magnetic Characterization</i>	44
4.3 Transmitter design and analysis.....	49
4.3.1 <i>Material selection of antenna</i>	49
4.3.2 <i>Experiment 1: The effect of shape of transmitter and the position of reciever</i>	50
4.4 Oil Recovery	54
4.4.1 <i>Experiment 1: Porosity and permeability test for glass beads sample</i>	54
4.4.2 <i>Experiment setup</i>	58
4.4.3 <i>Experiment 2: Oil recovery by using nanofluid injection</i>	60
4.4.4 <i>Experiment 3: Oil recovery by using electromagnetic wave tranmission and injection nanfluid</i>	66
 CHAPTER 5 CONCLUSION AND RECOMMENDATIONS	 76
5.1 Conclusion	76
5.2 Recommendations.....	77
REFERENCES	78

LIST OF FIGURES

Figure 1	Diagram of trapped oil in soil and rock.....	2
Figure 2	Water takes the path of least resistance when pumped into the ground.....	3
Figure 3	Electromagnetic wave propagation	10
Figure 4	Magnetic field lines of wire carrying current.....	11
Figure 5	Magnetic field of a circular loop.....	12
Figure 6	B-H curve for ferromagnetic material.....	15
Figure 7	Diagram of the forces on two molecules of liquid.....	17
Figure 8	Molecules at flat surface.....	18
Figure 9	Process Flow of the Project.....	19
Figure 10	Philip X-Ray Diffractometer.....	21
Figure 11	ZEISS Supra 55VP Field Emission Scanning Electron Microscope....	22
Figure 12	HP / AGILENT 4294A Precision Impedance Analyzer	23
Figure 13	Data acquisition system (DAS).....	24
Figure 14	Fluxgate magnetometer.....	24
Figure 15	Function generator 5MHz model Instek GFG-8250A.....	25
Figure 16	Balance Max 500g model Mettler Teledo.....	25
Figure 17	Masterflex console drive pump	26
Figure 18	Pressure gauge.....	26
Figure 19	Viscometer.....	27
Figure 20	Materials used.....	30

Figure 21	Stirring mixed solution for 24 hours	33
Figure 22	Gel formed	33
Figure 23	After drying	33
Figure 24	Crushing for 8 hours	33
Figure 25	Furnace for anneal the CoFe_2O_4 sample	34
Figure 26	Flow chart of Sample prepared by sol-gel method.....	35
Figure 27	XRD result for Cobalt Ferrite 600°C sample.....	37
Figure 28	XRD result for Cobalt 800°C sample.....	37
Figure 29	XRD Pattern for cobalt ferrite with [311] peak with annealed at temperature 600°C and 800°C	38
Figure 30	SEM image of cobalt ferrite, CoFe_2O_4 annealed at 600°C	40
Figure 31	SEM image of cobalt ferrite, CoFe_2O_4 annealed at 800°C	40
Figure 32	Spectrum and EDX data for cobalt ferrite, CoFe_2O_4 annealed at 600°C	42
Figure 33	Spectrum and EDX data for cobalt ferrite, CoFe_2O_4 annealed at 800°C	42
Figure 34	Procedure of making cobalt ferrite in toroid shape.....	44
Figure 35	Autopallet press machine.....	44
Figure 36	Cobalt ferrite in toroid shape with 20 turns winding.....	45
Figure 37	Initial permeability versus frequency for cobalt ferrite toroid.....	46
Figure 38	Q-factor versus frequency for cobalt ferrite toroid.....	46
Figure 39	Relative loss factor (RLF) versus frequency for cobalt ferrite.....	47
Figure 40	Glass beads mixture.....	54

Figure 41	Experiment setup.....	55
Figure 42	Schematic diagram experiment setup.....	58
Figure 43	Experiment setup.....	59
Figure 44	Brine collection for experiment 2.....	62
Figure 45	Oil collection for experiment 2.....	63
Figure 46	Oil recovered without EM wave transmission.....	65
Figure 47	Brine collection for experiment 3.....	68
Figure 48	Oil recovered by using EM wave transmission and injection nanofluid.....	70

LIST OF TABLES

Table 1	Material used for fabrication of Cobalt Ferrite	29
Table 2	Relative molecular mass for material used.....	32
Table 3	Calculations for CoFe_2O_4	32
Table 4	Standard Card of Cobalt Ferrite	36
Table 5	XRD data for 2 samples with different annealing temperatures	38
Table 6	EDX data and standard deviation for cobalt ferrite, CoFe_2O_4 at 600°C, and 800°C	43
Table 7	Properties of cobalt ferrite in toroid shape	45
Table 8	Conductivity of some common materials at 20°C.....	49
Table 9	Set up of straight shape transmitter	50
Table 10	Set up of curve shape transmitter	50
Table 11	Straight aluminium transmitter voltage and frequency profile	51
Table 12	Semi-circle aluminium transmitter voltage and frequency profile.....	52
Table 13	Glass Beads Mixture	54
Table 14	Measurement for permeability test.....	56
Table 15	Measurement for porosity test.....	57
Table 16	Calculation of percentage oil recovery for experiment 2	71
Table 17	Calculation of percentage oil recovery for experiment 3	73

CHAPTER 1

INTRODUCTION

1.1 Background of Study

Advanced technology explores ways to enhance the nation's energy resources. There are several challenges for deepwater field developments in order to meet the demand of oil and gas exploration. The oil production is carried out to three stages as listed below:

1. **Primary production**, in which the reservoir energy is used to produce oil and gas. During primary recovery, the natural pressure of the reservoir or gravity drive oil into the wellbore combined with artificial lift techniques (such as pumps) which bring the oil to the surface. But only about 10% of a reservoir's original oil in place is typically produced during primary recovery.

But petroleum isn't the only thing trapped in the earth. Water hides there too. Sooner or later, the reservoir begins producing water, along with oil, and it becomes uneconomical to extract them. The oil companies will then re-inject the water back into the reservoir. This stage of production is called secondary recovery.

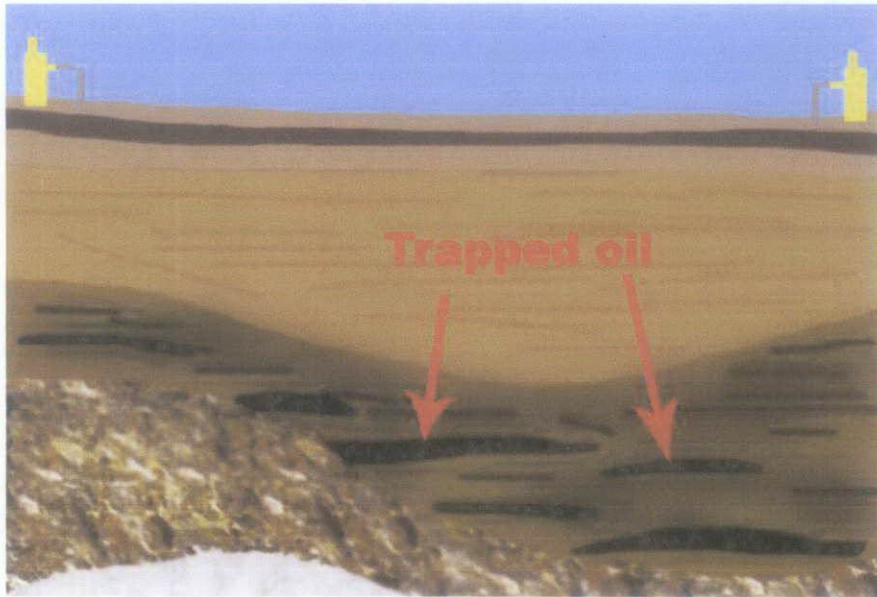


Figure 1: Diagram of trapped oil in soil and rock [1]

2. **Secondary recovery**, in which energy is given to the reservoir by injecting water or gas. Water injection helps maintain downhole pressure so that oil can continue to flow. Water from the injection well is also used to sweep or push the oil towards the producing wells. But rock in the reservoir has varying permeability. The more permeable the rock is, the more easily the fluid can flow through.

Unfortunately, water flows more readily than oil, and it always takes the path of least resistance. Once water creates a channel through the permeable rock to the producing wellbore, there is little benefit in injecting additional water. It only bypasses the oil instead of sweeping it ahead. The result is poor recovery from the reservoir.

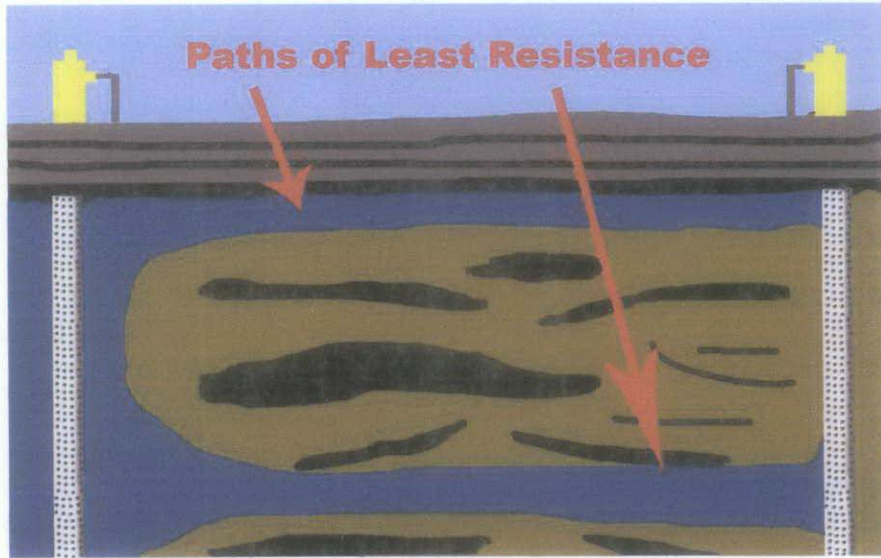


Figure 2: Water takes the path of least resistance when pumped into the ground[1]

3. **Enhanced Oil Recovery (EOR)** also called improved oil recovery or tertiary recovery. The purpose of EOR is to improve production, particularly in heavy oil reservoir. Using EOR, 30-60 %, or more, of the reservoir's original oil can be extracted compared with 20-40% using primary and secondary recovery [2].

Nowadays, researcher found that EM waves have big potential to be used as one of the EOR methods [3]. EM waves can be used in deep water because of its ability to propagate into the subsea surface to detect the presence of hydrocarbon reservoir. The characteristic of the EM waves that can penetrate deep through the reservoir be the main asset of why EM waves got potential to be used inside the reservoir [4]. This alternative method hopefully can maximize the crude oil production by at least with about 10% increment.

1.2 Problem Statement

Most wells produce complex, fractal drainage patterns that cause the oil to trap within the rocks. To recover the left oil (crude oil/heavy oil) from the reservoir is still remains as a challenge to the industry.

1.3 Objectives

The main objectives of this project are as follows:

- ✓ To synthesis and characterize the magnetic nanoparticles by using sol-gel method.
- ✓ To evaluate EM wave with magnetic nanoparticles can boost up the recovery percentage.

1.4 Scope of study

This project will be divided to 2 parts: i) Synthesis and characterize the magnetic nanoparticles. ii) Experiment on the effect of EM wave's diffusion to the core rock sample with the presence of magnetic nanoparticles. Thus, the scope of study covers for:

- ✓ Selection, synthesis and characterization of magnetic nanomaterial which is active reaction with EM wave.
- ✓ Validation the EM wave cooperates with the magnectic nanoparticles to reduce interfacial tension between oil-water interfaces to make the oil easily to flow.
- ✓ To calculate the oil recovery.

1.5 Feasibility of the project

This project is feasible to complete within the timeline which in 2 semesters. Universiti Teknologi PETRONAS (UTP) has enough equipments and facilities to do this project from the preliminary work until it is completed.

CHAPTER 2

LITERATURE REVIEW

2.1 Magnetic Nanoparticles

Magnetic nanoparticles are nanoparticle which can be manipulated using magnetic field. Such particles commonly consist of magnetic elements such as iron, nickel and cobalt [5]. These particles have been the focus of much research recently because they possess attractive properties which are high resistivity, low eddy current losses and high saturation magnetization. The physical and chemical properties of magnetic nanoparticles largely depend on the synthesis method and chemical structure. In most cases, the particles range from 1 to 100 nm in size [5].

Ferromagnetic cubic spinals namely ferrites possess properties of both magnetic materials and electric insulator. These properties make ferrites as an important material in many technological applications. These are preferred because of their high permeability in the radio frequency region, high electrical resistivity, mechanical hardness, chemical stability, etc. Their structural, electrical and magnetic properties depend on chemical composition, type and amount of dopant and method of preparation [6]. A bulk ferrite should have constant physical and magnetic properties regardless of its size, but for nanoscale materials this is not often the case and their properties will change as their size approaches to nanoscale.

John W. Dooley from Physics Department of Millersville University stated that magnetic polarization effects are similar to electric polarization effects. Just as electric dipole moments control the behavior of dielectric materials, magnetic dipole moments control the behavior of magnetic materials. An applied field causes the dipole moments to (partially) align, and the material is said to be polarized. This polarization produces a new field that adds to the applied field. Materials like iron, cobalt and nickel can retain their polarization after the applied magnetic field is turned off. These materials are said to be ferromagnetic. Ferromagnetic materials generally enhance an applied magnetic field, but their ability to hold a "permanent" polarization complicates the story. It is useful to think of ferromagnetism as a limiting case of paramagnetism, in which the substance is "polarized by its own field" [7].

Cobalt ferrite nanoparticles have recently become the subject of research interest from the point of view of the synthesis, the structure, the magnetic characterization, and the application. In particular, interest in cobalt ferrite powder as a ferromagnetic material has arisen due to its unique properties e.g. very high resistivity, a positive anisotropy constant, and a high magnetostriction which is defined as the change in the shape under the effect of magnetic field. These properties could make cobalt ferrite a potential candidate for many applications e.g. high frequency magnets, information storage systems, magnetic bulk cores, microwave absorbers and biomedical applications, such as magnetic hyperthermia, drug delivery, magnetic resonance imaging, and biosensors. Several techniques have been used to prepare Cobalt Ferrite nanoparticles. There are including the polymeric precursor method, sol gel, wet chemical routes, microemulsions, and chemical co-precipitation techniques [8]. In this project, cobalt ferrite nanoparticle is prepared by using sol-gel method.

2.2 Sol gel technique for preparation of the magnetic nanoparticles

Among the various existing methods of chemical synthesis, sol gel method is an alternative and promising technique for preparing soft ferrites, leading to highly pure, chemically homogeneous, and nanometric scale particles.

Sol-gel techniques have become very popular recently due to their high chemical homogeneity, low processing temperatures, and the possibility of controlling the size and morphology of particles. The sol-gel derived materials provide excellent matrices for a variety of organic and inorganic compounds. One of the most important features of doped sol-gel materials is their ability for preservation of chemical and physical properties of the dopants [9]. This sol-gel method also is an attractive technique for the preparation of nanosized particles because of the short processing time and potential to produce less expensive elements containing fiber alignment structures. The advantages of this method are the quality of the product can be controlled by ensuring the purity of the basic materials and the optical properties can be tailored by doping the basic materials or adding colloidal particle.

Nanoparticles exhibit a number special property relative to bulk material [10]. For this reason, there are new techniques to produce particles of different nanosizes with a good grade of homogeneity. Several techniques have been used for the preparation of nanoparticles. These include coprecipitation, hydrothermal, sol gel, high energy milling, etc. Solution methods, particularly the sol-gel and self combustion, have overcome the problem of improving or increasing the performance of the substituted the nanoparticles.

2.3 Electromagnetic Wave for EOR

Electromagnetic is created by the vibration of an electrical charge. This vibration creates a wave which has both an electric and a magnetic component. An electromagnetic wave transports its energy at a speed of 3×10^8 m/s through a vacuum. While the propagation of an electromagnetic wave through a material medium occurs at net speed which less than 3×10^8 m/s.

Chakma and Jha (1992) reported that the presence of water is essential in the oil-bearing zone for continuous propagation of electromagnetic energy. The further study mentioned that the presence of higher salinity increase the conduction of the electromagnetic wave. However, very high thickness of bottom water may result in huge heat loss, causing the efficiency of the system. The study reported the yield of 45% of oil initially in place of heavy oil of moderate viscosity was recovered [11].

According to Amit Chakma et al (1992), the utilization of electrical energy for example can also be described as electromagnetic, where electromagnetic energy is delivered at low frequency. On the other end of the electromagnetic spectrum, microwave ovens that employ high frequencies also used electromagnetic energy [11].

The using of electromagnetic system on recovery of heavy oil reservoirs containing a bottom-water zone have be done by Islam, M. R., and Chakma, A. (1992), researcher from Alaska. They reported that electromagnetic wave transmission system is practically limited to small radius but becomes effective in combination with horizontal wells. It was further reported that the recovery can be enhanced by coupling the electromagnetic wave transmission system with gas or water injection in order to create the favorable pressure gradient in the presence of

bottom water. The model showed that a recovery as high as 77% of oil in place (OIP) was obtained [12].

Theory:

Electromagnetic (EM) wave is a self-propagation wave in space or through matter. EM wave has an electric field (E) and magnetic field (B) component which oscillate in phase perpendicular to each other and to the direction of energy propagation. Figure 3 shows the electromagnetic wave propagation. EM wave is classified into type according to the frequency of the wave. These types include radio waves, microwaves, terahertz radiation, infrared radiation, visible light, ultraviolet radiation, X-ray and gamma rays. EM wave carries energy and momentum, which may be imparted when it interacts with matter [13].

Electric field generates a magnetic field and vice versa. Therefore, as oscillating electric field generates an oscillating magnetic field, the magnetic field in turn generates an oscillating electric field, and so on. These oscillating fields together form an electromagnetic wave.

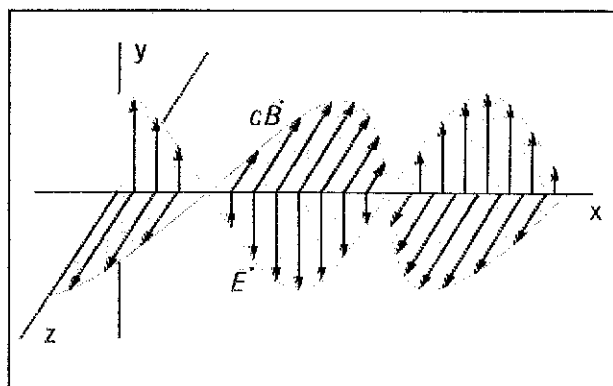


Figure 3: Electromagnetic Waves propagation [14]

The magnetic field lines around a long wire which carries an electric current form concentric circles around the wire. The direction of the magnetic field is perpendicular to the wire and is in direction the fingers of your right hand would curl if you wrapped them around the wire with your thumb in the direction of the current [15]. Figure 4 shows the magnetic field lines induced by a wire carrying current.

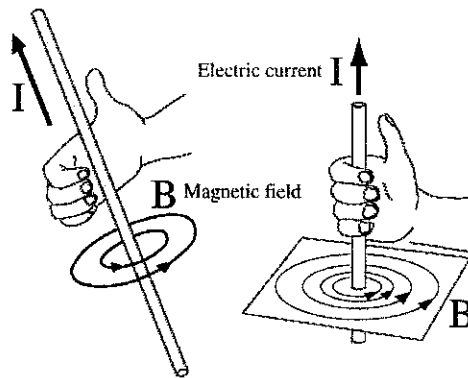


Figure 4: Magnetic field lines of wire carrying current [16]

Maxwell equation stated that the magnetic field produced magnetic field (B) is proportionally related to the current and the type of material used. The bigger current flow inside a conductor, and the higher the permeability of the material used, the bigger B field is produced.

Based on Maxwell equation [17],

$$B = \frac{\mu_0 I}{2\pi r} \quad (1)$$

Where;

B = Magnetic field

μ_0 = Permeability

I = Current

r = Distance

Electric current in a loop creates a magnetic field which is more concentrated in center of the loop [15]. Figure 5 show the magnetic field of a circular loop.

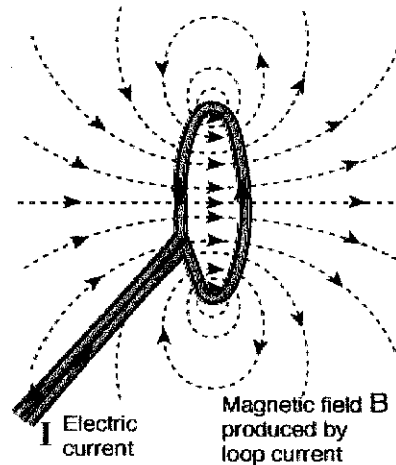


Figure 5: Magnetic field of a circular loop [18]

The magnetic field at the center of the circular loop from Bio- Savart law is

$$B = \frac{\mu_0 I}{2R} \quad (2)$$

Where;

B = Magnetic field

μ_0 = Permeability of free space

I = Current

R = Loop radius

Electric and magnetic wave's field also may exist in space without a material medium being present and if they vary in space and time in the appropriate way, the spatial variation will propagate as a wave, transporting energy.

2.4 Electromagnetic Transmitter

EM transmitter is defined as a radial waveguide that generates the EM waves [21]. It is a device where use turns of coil to generate the electromagnetic wave that is at a single frequency. When we apply a high frequency source of alternating voltage input to the coils/winding of the transmitter, a magnetizing current is developed in the winding itself. This magnetizing current then will generate an alternating flux in the magnetizable core that links the winding in order to develop an alternating polarity output voltage [20].

Generally, antennas that radiate electric field have two components insulated from each other. The simplest electric field antenna is the dipole antenna, whose very name implies its two-component nature. The two conductor elements act like the plates of a capacitor with the field between them projecting out into space rather than being confined between the plates. On the other hand magnetic field antennas are made of coils which act as inductors. The inductor fields are projected out into space rather than being confined to a closed magnetic circuit.

2.4.1 Radiation Pattern

Radiation pattern is defined as mathematical function or a graphical representation of the radiation properties of the antenna as a function of space coordinates. Radiation properties include power flux density, radiation intensity, field strength, directivity phase or polarization [13].

2.4.2 Directivity

Directivity is defined as the ratio of the radiation intensity in a given direction from the antenna to radiation intensity averaged over all directions. The average radiation intensity is equal to the total power radiated by the antenna divided by 4π .

$$D = 4\pi \frac{U}{P_{rad}} \quad (3)$$

Where;

D = Directivity

U = Radiation intensity (W/unit solid angle)

P_{rad} = Total radiated power (W)

2.4.3 Gain

Gain is a useful measure to describe the performance of an antenna. It takes into account the efficiency of the antenna as well as its directional capabilities. It is defined as the ratio of the radiation intensity of an antenna in a given direction, to the intensity of the same antenna as it radiates in all directions (isotropically). The gain of antenna is a passive phenomenon. Power is not added by the antenna, but simply redistributed to provide more radiated power in a certain direction than would be transmitted by an isotropic antenna. If an antenna has a positive gain energy is conserved by the antenna.

2.4.4 Efficiency

The total antenna efficiency is used to take into account losses as the input terminals and within the structure of the antenna.

2.5 Magnetic saturation

For magnetic materials, saturation is the state when the material cannot absorb a stronger magnetic field, such that an increase of magnetization produces no significant change in magnetic flux density. So, the total flux density, B , levels off. Saturation is most clearly seen in the magnetization curve. Figure 6 shows the magnetization curve or also known as B-H curve for sheet steel, cast steel and cast iron.

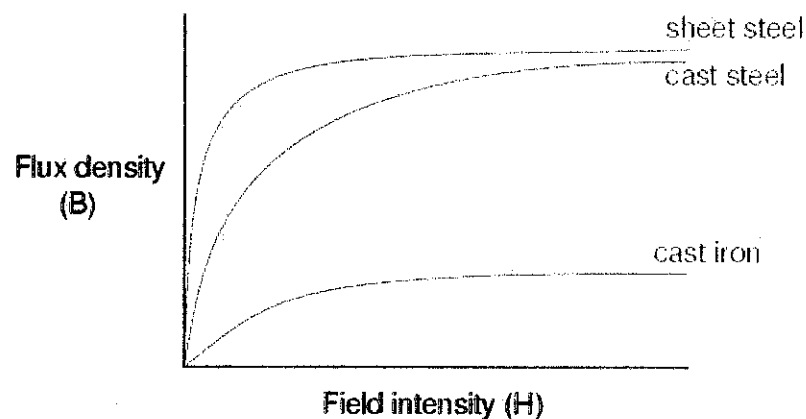


Figure 6: B-H curve for ferromagnetic material [21]

From Figure 6, it can be noticed how the flux density for any of the above materials (cast iron, cast steel, and sheet steel) levels off with the increasing amounts of field intensity. When there is little applied magnetic force, low H , only a few atoms are in alignment, and the rest are easily aligned with additional force. However, as the external field increases further, more flux gets crammed into the same cross-sectional area of a magnetic material [21]. Fewer atoms are available within that material to align their electrons with the additional force, therefore, the slope of the curve decrease. At some point, all electrons will be aligned with the external magnetic field. Any increase in the magnetic field will not increase the magnetization [22].

2.6 Permeability

Permeability is the degree of magnetization of a material that responds linearly to an applied magnetic field. Magnetic permeability is typically represented by the letter μ . Magnetic permeability, μ , of a particular material is defined as the ratio flux density to magnetic field strength:

$$\mu = \frac{B}{H} \quad (4)$$

Where;

μ = Permeability

B = Magnetic flux density

H = Magnetic field strength

Relative permeability C_r , is the ratio of the permeability of a specific medium to the permeability of free space given the magnetic constant $\mu_0 = 4\pi \times 10^{-7}$ H/m.

$$\mu_r = \frac{\mu}{\mu_0} \quad (5)$$

Where;

μ_r = Relative permeability

μ = Permeability of medium

μ_0 = Permeability of free space

2.7 Interfacial Tension

The interfacial tension of immiscible liquids is an important physical property that is useful in determining the behavior of liquids in such diverse areas as dispersions, emulsions, and enhanced oil recovery processes [23]. Interfacial tension is somewhat similar to surface tension in that cohesive forces are also involved. However the main forces involved in interfacial tension are adhesive forces (tension) between the liquid phase of one substance and either a solid, liquid or gas phase of another substance. The interaction occurs at the surfaces of the substances involved, that is at their interfaces [24].

When two different phases (gas/liquid, liquid/liquid, gas/solid or liquid/solid) are in contact with each other the molecules at the interface experience an imbalance of forces. This will lead to an accumulation of free energy at the interface. The excess energy is called surface free energy and can be quantified as a measurement of energy/area i.e. the energy required to increase the surface area of the interface by a unit amount. It is also possible to describe this situation as having a line tension or interfacial tension (IFT), which is quantified as a force/length measurement. This force tends to minimize the area of the surface. This excess energy exists at any interface. If one of the phases is the gas phase of a liquid being tested, the measurement is normally referred to as Surface Tension (ST). If the surface investigated is the interface of two immiscible liquids the measurement is normally referred to as interfacial tension (IFT) [25].

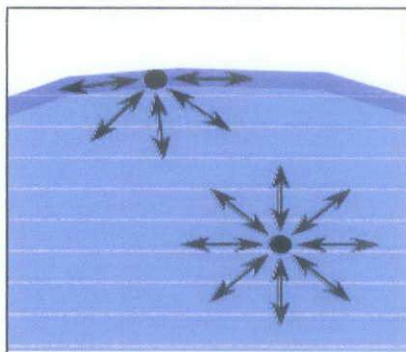


Figure 7: Diagram of the forces on two molecules of liquid [26].

In the bulk of the liquid, each molecule is pulled equally in every direction by neighboring liquid molecules, resulting in a net force of zero. The molecules at the surface do not have other molecules on all sides of them and therefore are pulled inwards. This creates some internal pressure and forces liquid surfaces to contract to the minimal area. The interfacial tension of pure oil/water systems can be altered by adding another organic liquid to the oil phase, resulting in compositional change at the interface and hence changes in the cohesive and adhesive forces [23].

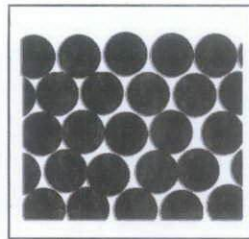


Figure 8: Molecules at flat surface [26].

Mundimex companies have introduced a device, Magnetizer's Oil Line Energizers, which is used to alter the electrical potential of crude, which change its nature and retard and reduce deposition of crude oil. As it passes through the monopole magnetic field of the devices, the crude's potential is altered causing its chemical, mechanical and electrical properties to change. This eliminates the crystal process at the thermal or cloud point and the transformation of crude oil from liquid to a solid-state ceases. This reduces the surface tension and the viscosity of crude. By controlling the surface tension of the crude, the paraffin are kept in solution, rather than adhering to each other [27].

CHAPTER 3

METHODOLOGY

3.1. Procedure Identification

Figure 9 below describe the flow chart of this project and will implemented throughout the time.

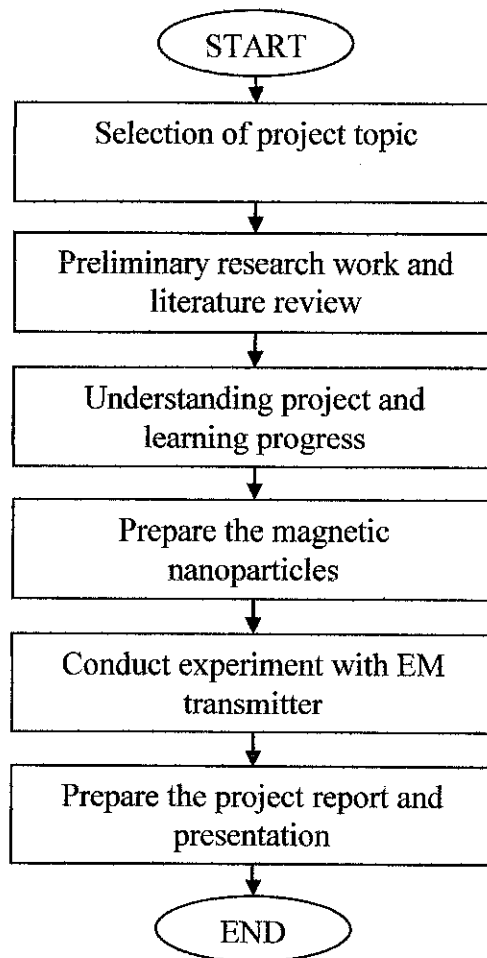


Figure 9: Process Flow of the Project

The first step is to select the project topic and conduct the preliminary researches and literature review. Journals, conference papers, books and internet are referred. As the information is available, it is very crucial for the author to undergo the learning process as the enhanced oil recovery (EOR) is not a familiar area. From the data gathered, the author gets the basic understanding what the project is all about.

The next step is development magnetic nanoparticles which are will be used as the medium to absorb EM waves and to reduce interfacial tension between oil-water interfaces to make the oil easily to flow and to control mobility of the reservoir fluids, respectively and at the same time assist the oil recovery from the glass beads pack. The selection of the material use for the magnetic nanoparticles is very important in order to satisfy the project objective which is to maximize the oil production.

Next is to conduct experiment of oil recovery using EM method with presence of magnetic nanoparticles. Data gathered from the experiment will be analyze and proceed for a proper reporting to the Final Year Project Committee. There is also an oral presentation which will take place towards the end of the semester.

3.2. Tools Required

Software and hardware which are required for completing this project are listed below:

3.2.1 X-Ray Diffraction (XRD)

X-ray scattering techniques are a family of non-destructive analytical techniques which reveal information about the crystallographic structure, chemical composition, and physical properties of materials and thin films. These techniques are based on observing the scattered intensity of an X-ray beam hitting a sample as a function of incident and scattered angle, polarization, and wavelength or energy.

X-ray diffraction finds the geometry or shape of a molecule using X-rays. X-ray diffraction techniques are based on the elastic scattering of X-rays from structures that have long range order. The most comprehensive description of scattering from crystals is given by the dynamical theory of diffraction [28].

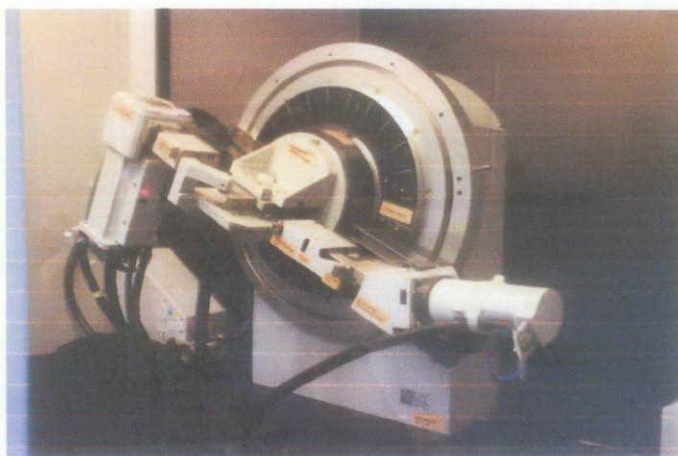


Figure 10: Philips X-Ray Diffractometer [29]

3.2.2 *Field Emission Scanning Electron Microscope (FESEM)*

A field-emission cathode in the electron gun of a scanning electron microscope provides narrower probing beams at low as well as high electron energy, resulting in both improved spatial resolution and minimized sample charging and damage. The application of FESEM include Semiconductor device cross section analyses for gate widths, gate oxides, film thicknesses, and construction details, advanced coating thickness and structure uniformity determination and small contamination feature geometry and elemental composition measurement. FESEM is needed because of;

- i. FESEM produces clearer, less electrostatically distorted images with spatial resolution down to 1 1/2 nm. That's 3 to 6 times better than conventional SEM.
- ii. Smaller-area contamination spots can be examined at electron accelerating voltages compatible with Energy Dispersive X-ray Spectroscopy.
- iii. Reduced penetration of low kinetic energy electrons probes closer to the immediate material surface.
- iv. High quality, low voltage images are obtained with negligible electrical charging of samples. (Accelerating voltages range from 0.5 to 30 kV.)
- v. Need for placing conducting coatings on insulating materials is virtually eliminated [30].



Figure 11: ZEISS Supra 55VP Field Emission Scanning Electron Microscope [31]

3.2.3 Energy Dispersive X-ray spectroscopy (EDX)

Energy dispersive X-ray spectroscopy (EDX) is an analytical technique used for the elemental analysis or chemical characterization of a sample. It is one of the variants of XRF. As a type of spectroscopy, it relies on the investigation of a sample through interactions between electromagnetic radiation and matter, analyzing x-rays emitted by the matter in response to being hit with charged particles. Its characterization capabilities are due in large part to the fundamental principle that each element has a unique atomic structure allowing x-rays that are characteristic of an element's atomic structure to be identified uniquely from each other [32].

3.2.4 LCR vector network analyzer

HP / AGILENT 4294A Precision Impedance Analyzer 40 to 110 MHz is used to get the data for the initial permeability and Q-factor for the respective toroids.



Figure 12: HP / AGILENT 4294A Precision Impedance Analyzer

3.2.5 Hardware required

- Transmitter

Transmitter is used to transmit the electromagnetic waves.

- Decaport data acquisition system (DAS) Model NI PXI-1042 and Fluxgate Magnetometer

Fluxgate Magnetometer was used in order to detect EM waves and DAS is used to store the data of the transmitted EM waves.

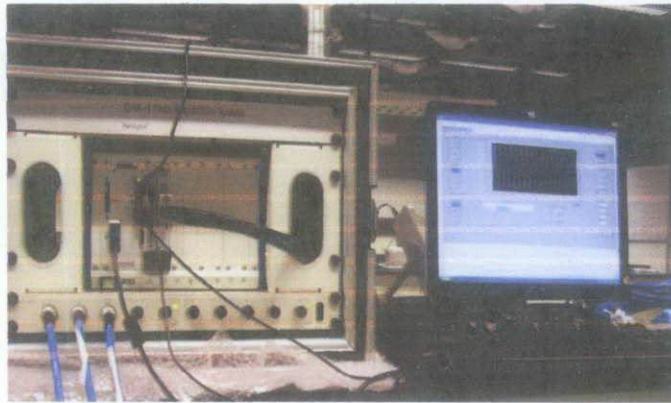


Figure 13: Data acquisition system (DAS)

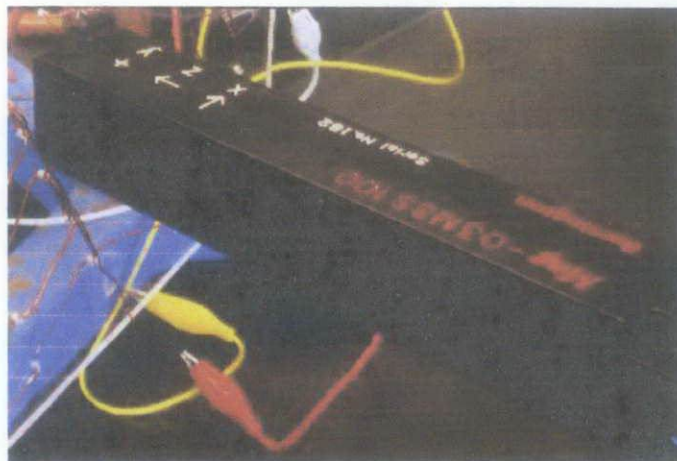


Figure 14: Fluxgate magnetometer

- Function generator

Function generator was used to supply 1 KHz frequency to transmitter and magnetic feeder.



Figure 15: Function generator 5MHz model Instek GFG-8250A

- Balance

Balance was used to weigh the materials and glass beads sample. It gives accurate reading up to 4 decimal points.

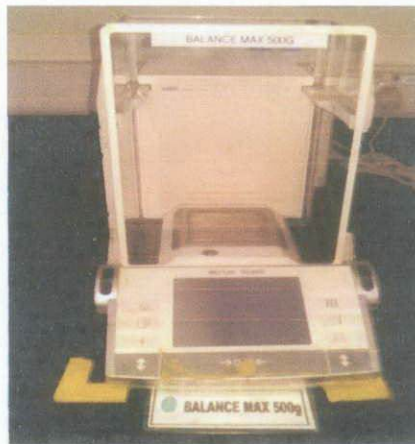


Figure 16: Balance Max 500g model Mettler Teledo

- Masterflex console drive pump

Masterflex console drive pump is used to flow the brine to the cylindrical PVC column. The flow of the brine out form the outlet of the pump has been test for constant flow rate, 2ml/min.



Figure 17: Masterflex console drive pump

- Pressure gauge

Pressure gauge is used to record the pressure value during permeability and porosity test. The pressure is measured for every 10 minutes and until reach the constant pressure. Constant pressure means steady state condition is achieved.



Figure 18: Pressure gauge

- Viscometer

Viscometer was used to measure the viscosity of water, brine and oil.



Figure 19: Viscometer

Below is the simplified procedure for using viscometer.

- 1) Turn the power ON using the switch located on the near of the base console. The main screen will be displayed.
P = poise (unit)
RPM = rotation per minute
- 2) Select and attach the cone.
- 3) Set the temperature control.
- 4) Set the cone number.
- 5) Set the speed of rotation.
- 6) Lower the handle placing the cone onto the plate. Lock the handle into as lowest position. Allow around ten minutes for the cone to come to equipment temperature with the plate.
- 7) Raise the handle. Place the sample to be measured onto the plate below the cone. Lower the handle gently. Do not force the cone onto the plane. The sample must completely down the face of the cone and extend beyond the edge of the cone about 1.0mm.
- 8) Allow the cone, plate and sample to equilibrate to the temperature control setting.

- 9) Set the RUN TIME for rotating the cone.
- 10) Press the RUN key and execute the viscosity measurement.
- 11) Read the result of the sample treat.
- 12) Remove the cone for clearing
- 13) Clean the viscometer plate

CHAPTER 4

RESULTS AND DISCUSSIONS

4.1 Synthesis of Cobalt Ferrite

This project focuses cobalt ferrite powder as magnetic nanoparticles using the sol-gel process. A particular emphasis is devoted to the understanding of the role of the chemical parameters involved in the sol-gel technique, and of the heat treatment on the structures and morphologies of the materials obtained.

4.1.1 Experimental Procedure

Table below shows the material used for the fabrication of Cobalt Ferrite, CoFe_2O_4 .

Table 1: Material used for fabrication of Cobalt Ferrite.

No.	Material
1	Cobalt (II) Nitrate Hexahydrate [$\text{Co}(\text{NO}_3)_2 \cdot 6\text{H}_2\text{O}$]
2	Iron (III) Nitrate Nanohydrate [$\text{Fe}(\text{NO}_3)_3 \cdot 9\text{H}_2\text{O}$]
3	Nitric Acid [HNO_3]

All metal nitrates used in the fabrication of Cobalt Ferrite, CoFe_2O_4 were dissolved in the aqueous solution of 165 ml nitric acid HNO_3 . Following calculations is done in order to prepare 20g of CoFe_2O_4 by using sol gel technique. Details of the calculations are simplified in table 3.

4.1.2 Calculation of Cobalt Ferrite, CoFe_2O_4 using sol-gel method

Starting materials are Cobalt (II) Nitrate Hexahydrate [$\text{Co}(\text{NO}_3)_2 \cdot 6\text{H}_2\text{O}$], and Iron (III) Nitrate Nanohydrate [$\text{Fe}(\text{NO}_3)_3 \cdot 9\text{H}_2\text{O}$].



Figure 20: Materials used

- Balance equation:



Relative molecular mass for Cobalt (II) Nitrate Hexahydrate

I. $\text{Co}(\text{NO}_3)_2 \cdot 6\text{H}_2\text{O}$ (considering H_2O)

$$= 58.9332 + (2 \times 14.0067) + (12 \times 15.9994) + (12 \times 1.0079)$$

$$= 58.9332 + 28.0134 + 191.9928 + 12.0948$$

$$= 291.0342 \text{ g/mol}$$

II. $\text{Co}(\text{NO}_3)_2$ (without considering H_2O)

$$= 58.9332 + (2 \times 14.0067) + (6 \times 15.9994)$$

$$= 58.9332 + 28.0134 + 95.9964$$

$$= 182.9430 \text{ g/mol}$$

Relative molecular mass for Iron (III) Nitrate Nanohydrate

I. $\text{Fe}(\text{NO}_3)_3 \cdot 9\text{H}_2\text{O}$ (considering water)

$$= 55.8450 + (3 \times 14.0067) + (18 \times 15.9994) + (18 \times 1.0079)$$

$$= 55.8450 + 42.0201 + 287.9892 + 18.1422$$

$$= 403.9965 \text{ g/mol}$$

II. $\text{Fe}(\text{NO}_3)_3$ (without water)

$$= 55.8450 + (3 \times 14.0067) + (9 \times 15.9994)$$

$$= 55.8450 + 42.0201 + 143.9946$$

$$= 241.8597 \text{ g/mol}$$

- To prepare 20g of CoFe_2O_4

Table 2: Relative molecular mass for material used

Material	Relative molecular mass (Without water)	Relative molecular mass (With water)
$\text{Co}(\text{NO}_3)_2$	182.9430 g/mol	291.0342 g/mol
$2\text{Fe}(\text{NO}_3)_3$	(2 x 241.8897) = 488.7208 g/mol	(2 x 403.9965) = 807.9930 g/mol
Total	666.6638 g/mol	1099.0272 g/mol

Mass of salt needed without water

$$\text{Co}(\text{NO}_3)_2 = \frac{182.9430 \text{ g/mol}}{666.6638 \text{ g/mol}} \times 20 \text{ g} = 5.4883 \text{ g}$$

$$2\text{Fe}(\text{NO}_3)_3 = \frac{488.7208 \text{ g/mol}}{666.6638 \text{ g/mol}} \times 20 \text{ g} = 14.5117 \text{ g}$$

Mass of hydrated salt needed with water

$$\text{Co}(\text{NO}_3)_2 \cdot 6\text{H}_2\text{O} = \frac{291.0342 \text{ g/mol}}{182.9430 \text{ g/mol}} \times 5.4883 \text{ g} = 8.7310 \text{ g}$$

$$2\text{Fe}(\text{NO}_3)_3 \cdot 9\text{H}_2\text{O} = \frac{807.9930 \text{ g/mol}}{488.7208 \text{ g/mol}} \times 14.5117 \text{ g} = 24.2399 \text{ g}$$

Table 3: Calculations for CoFe_2O_4

Material	Weight (without water)/g	Final weight (with water)/g
$\text{Co}(\text{NO}_3)_2$	5.4883 g	8.7310 g
$2\text{Fe}(\text{NO}_3)_3$	14.5117 g	24.2399 g
Total	20.0000 g	32.9709 g

The solutions were stirred at 250 r.p.m for 1 day separately and then were mix into one solution. Then, the mixture was stirred for another 1 day and then heated up gradually at 40°C, 50°C, 60°C and 70°C until gel-like solution was formed and the heating process is stopped immediately.



Figure 21: Stirring mixed solution for 24 hours

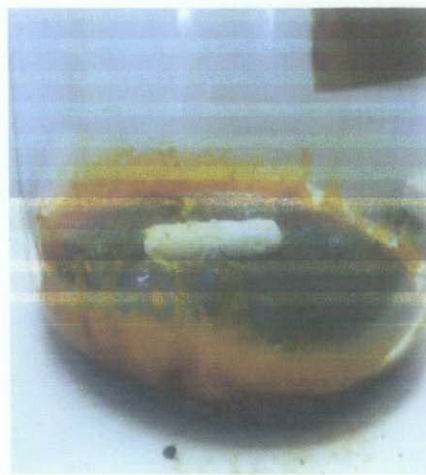


Figure 22: Gel formed

Then, the samples were dried in an oven at 110°C for 10 days for evaporation purpose. After that, the dried samples were crushed for 8 hours to obtain fine particles.



Figure 23: After drying



Figure 24: Crushing for 8 hours

Then, powder sintered at 600 °C and 800 °C for 4 hours to get the required characteristics of ferrite powder.



Figure 25: Furnace for anneal the CoFe_2O_4 sample

After annealing process is complete, the samples were crushed again for 2 hours. Then, these samples were characterized using X-Ray Diffractions (XRD), Field Emission Scanning Electron Microscope (FESEM) and Energy Dispersive X-Ray (EDX).

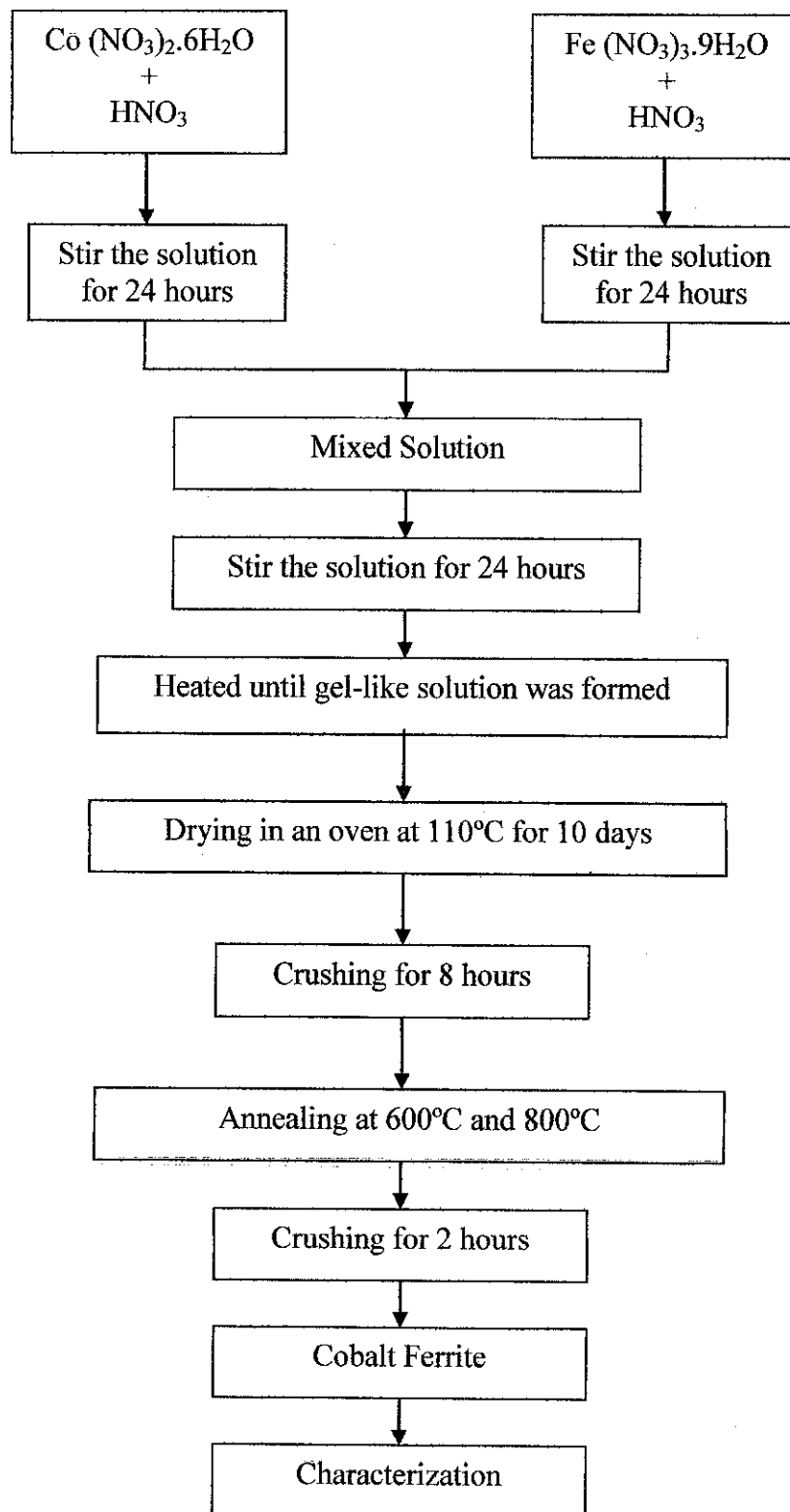


Figure 26: Flow chart of Sample prepared by sol-gel method

4.2 Characterization of Cobalt Ferrite

4.2.1 X-Ray Diffraction (XRD) Results

The result gathered from the XRD is matched with the standard card of Cobalt Ferrite. Refer to Table 4.

Table 4: Standard Card of Cobalt Ferrite

SAMPLE	STANDARD CARD
CoFe ₂ O ₄ (600 ^o C)	SS-NNNN 79-1744 (C)
CoFe ₂ O ₄ (800 ^o C)	SS-NNNN 79-1744 (C)

By applying Scherer equation the average crystallite size of the particles can be calculated. The Scherer's equation is [33]:

$$D = \frac{K\lambda}{\beta \cos\theta} \quad (6)$$

Where:

K = 0.9

λ = X-ray wavelength (1.5408 Åm)

β = FWHM 2 θ

θ = Bragg's angle

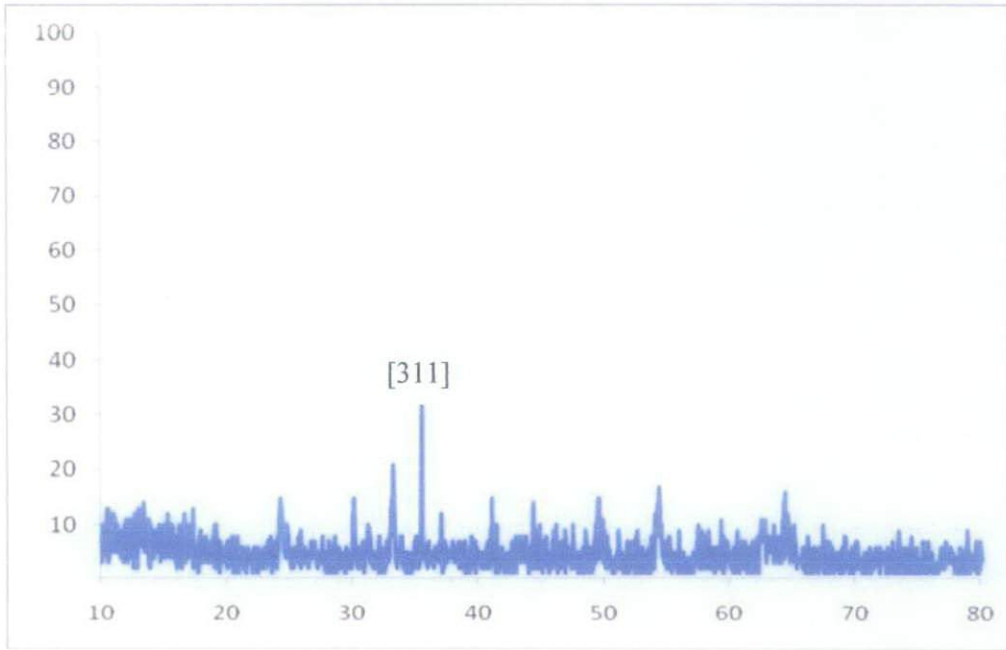


Figure 27: XRD result for Cobalt Ferrite 600°C sample

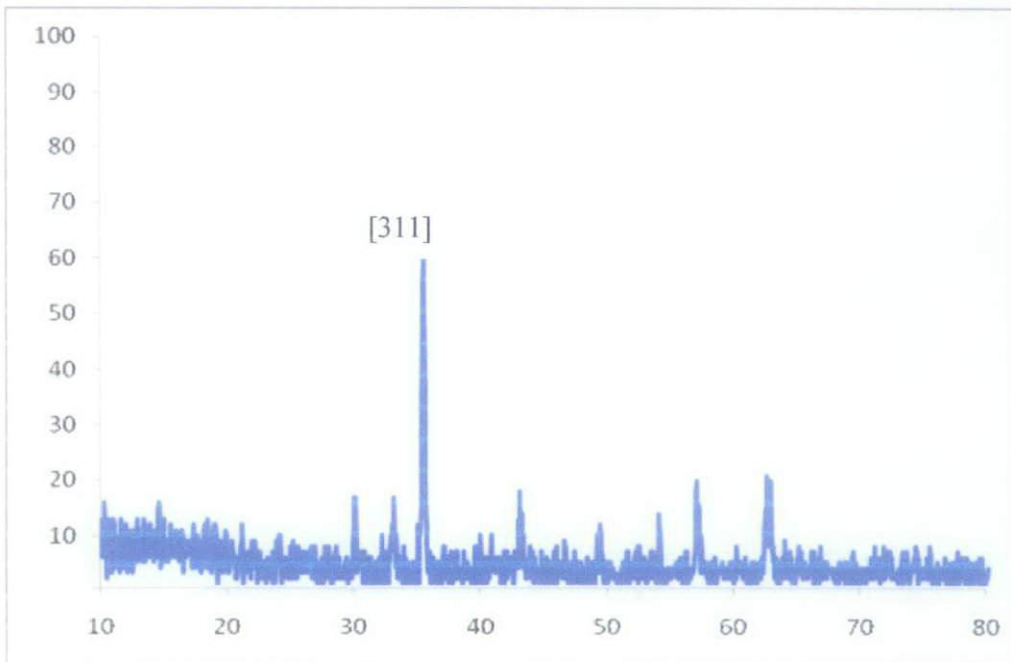


Figure 28: XRD result for Cobalt Ferrite 800°C sample

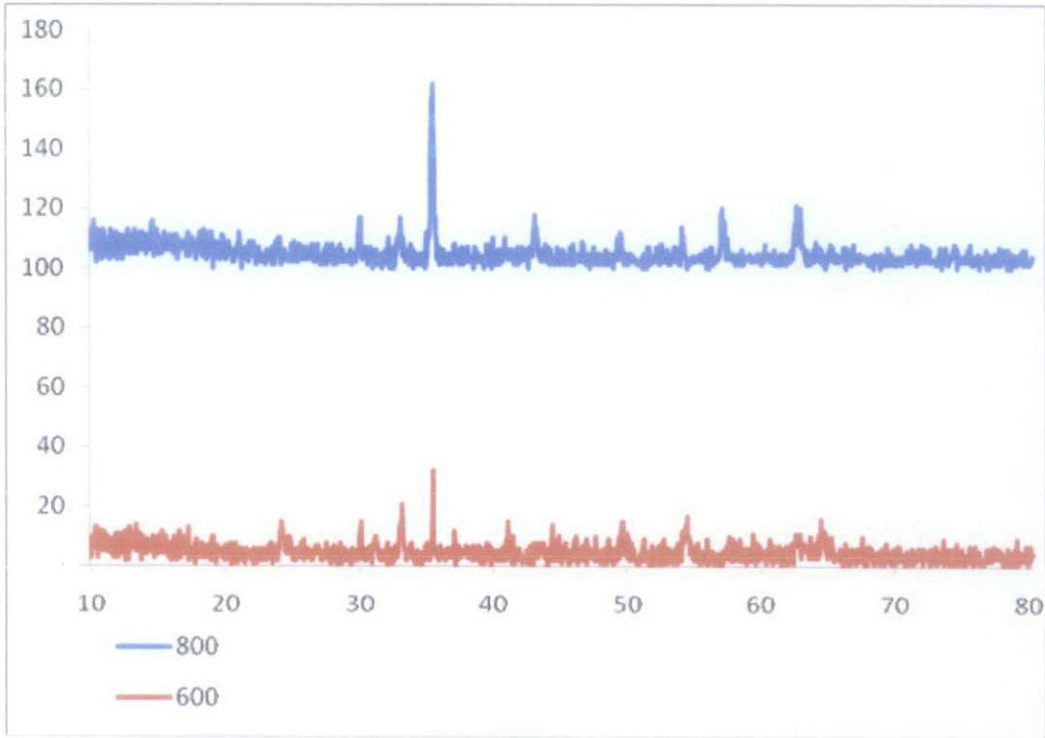


Figure 29: XRD Pattern for Cobalt Ferrite with [311] peak with annealed at temperature 600°C and 800°C.

Table 5: XRD data for 2 samples with different annealing temperatures

Samples	X-Ray Diffraction (Correspond to [311] peaks)						
	Intensity (Counts)	FWHM	d-spacing (Å)	Crystallite size (nm)	a	b	c
600°C	32	0.256	2.69023	5.4170	5.9366	5.9366	14.543
800°C	62	0.271	2.53191	5.1171	5.9366	5.9366	14.543

Discussion:

Table 5 shows the XRD analysis which identifies the value of full width half maxima (FWHM), d-spacing and crystallite size for the [311] plane as a high peak. Scherer's equation is used to determine the diameter of Cobalt Ferrite nanoparticles by using XRD results.

From the table, it is clear that as we increase the annealing temperature from 600 °C to 800°C the crystallite size decreases and also lattice parameter decreases. However, we don't know the exact temperature when the crystallite size will increase since experiment is conducted for only two temperatures and not for every temperature. Cobalt Ferrite powder which anneal at 1200°C where we expect the crystallite size will increase. Besides that, based on standard card, Cobalt Ferrite gives Hexagonal structure. By applying Scherer equation 800°C sample gives smaller crystallite size and higher intensity which are 5.1171nm and 62 respectively.

4.2.2. Field Emission Scanning Electron Microscope (FESEM) Results

The morphology of the materials (particles size) was observed by a field emission-scanning electron microscope (FESEM). Figure 31 and 32 shows the morphology for Cobalt Ferrite, CoFe_2O_4 annealed at 600°C , and 800°C respectively.

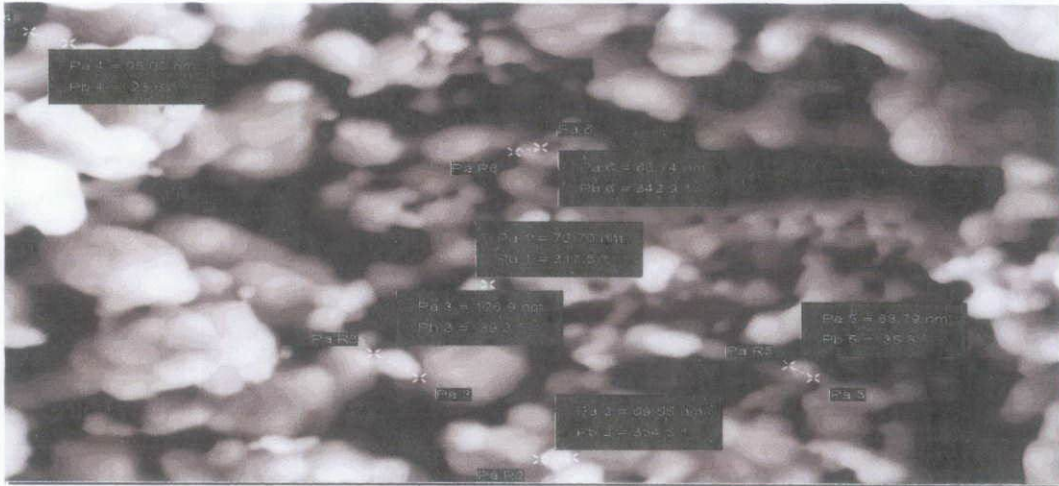


Figure 30: SEM image of Cobalt Ferrite, CoFe_2O_4 annealed at 600°C

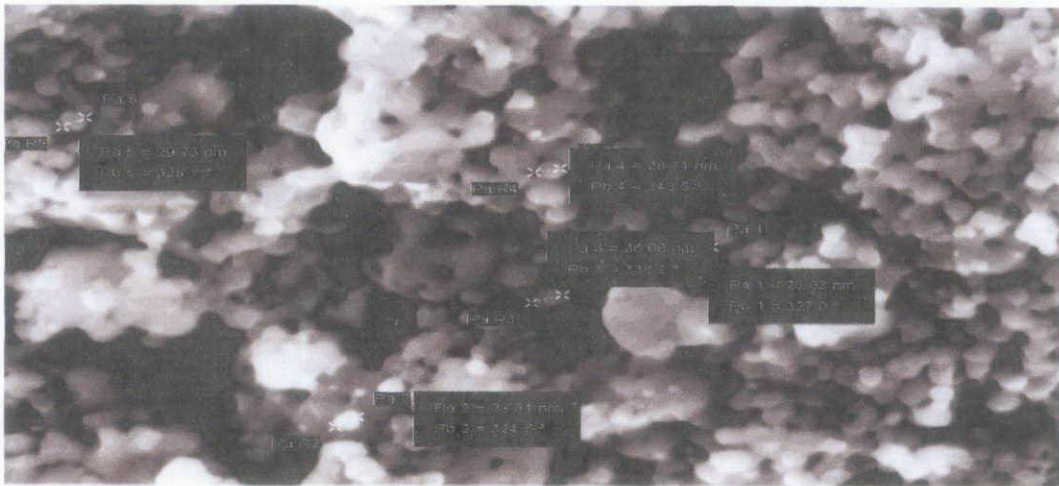


Figure 31: SEM image of Cobalt Ferrite, CoFe_2O_4 annealed at 800°C

Discussion:

For sample annealed at 600°C, the particle size in the range of 60nm to 127nm. The second sample which annealed at 800 °C, the particle size in the range of 26nm to 36nm. Results show that the grain size is decreasing as the sintering temperature increases.

4.2.3 Energy Dispersive X-Ray (EDX)

Energy Dispersive X-Ray (EDX) is a chemical microanalysis technique performed in conjunction with FESEM. Figures below shows that the atomic and weight percentage of the corresponding elements which are Cobalt, Ferum and Oxygen.

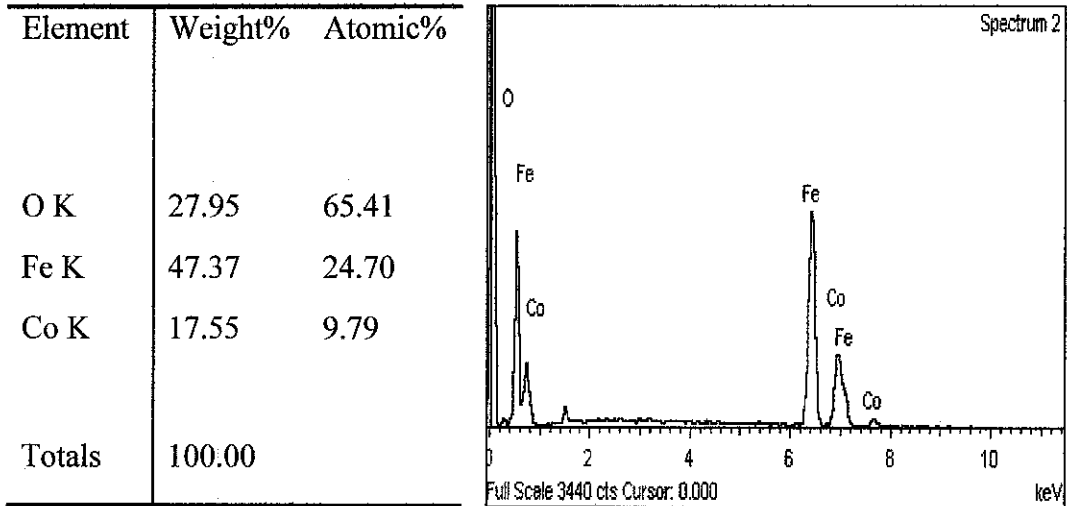


Figure 32: Spectrum and EDX data for Cobalt Ferrite, CoFe_2O_4 annealed at 600°C

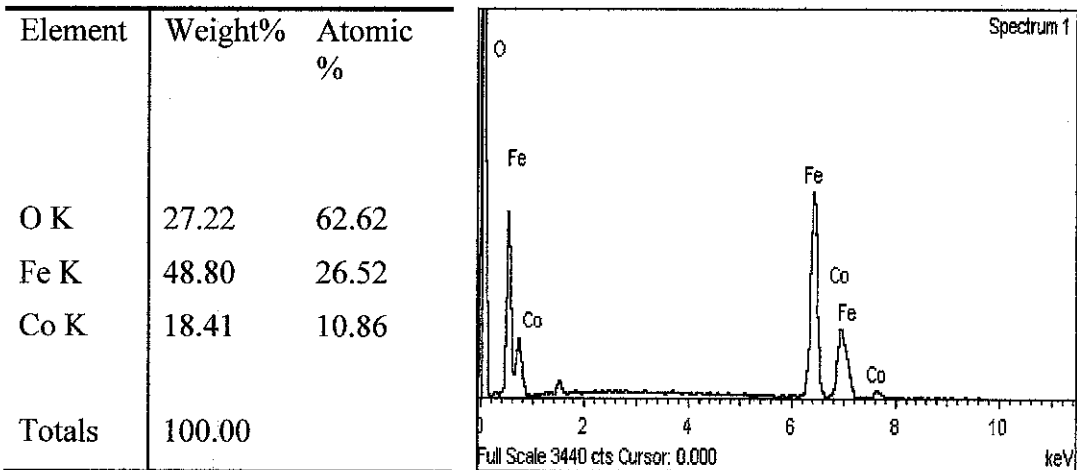


Figure 33: Spectrum and EDX data for Cobalt Ferrite, CoFe_2O_4 annealed at 800°C

Theoretical value of atomic in percent (%) for Cobalt Ferrite, CoFe_2O_4 is calculated as below.

$$\text{CoFe}_2\text{O}_4 = 7$$

$$\text{Co} = \frac{1}{7} \times 100\% = 14.29\%$$

$$\text{Fe} = \frac{2}{7} \times 100\% = 28.57\%$$

$$\text{O} = \frac{4}{7} \times 100\% = 57.14\%$$

Table 6: EDX data and standard deviation for cobalt ferrite, CoFe_2O_4 at 600°C, and 800°C .

Samples			600° C	800 °C
Elements				
Co	Weight (%)		17.55	18.41
	Atomic (%)		9.79	10.86
	Standard deviation (%)		31.49	24.00
Fe	Weight (%)		47.37	48.80
	Atomic (%)		24.70	26.52
	Standard deviation (%)		13.55	7.18
O	Weight (%)		27.95	27.22
	Atomic (%)		65.41	24.96
	Standard deviation (%)		14.47	9.59

Discussions:

Experimental atomic value is compared with the theoretical atomic value. Cobalt ferrite sample anneal at 800°C is chosen because it has lower standard deviation of Co, Fe, and O which are 24%, 7.18% and 9.59% respectively.

4.2.4 Magnetic Characterization

Objective: To analyze the initial permeability, Q-factor and relative loss factor (RLF) for cobalt ferrite powder.

Cobalt ferrite powder was fabricated in the form of toroid in order to analyze the magnetic characterization. Below is the procedure to make the toroid:

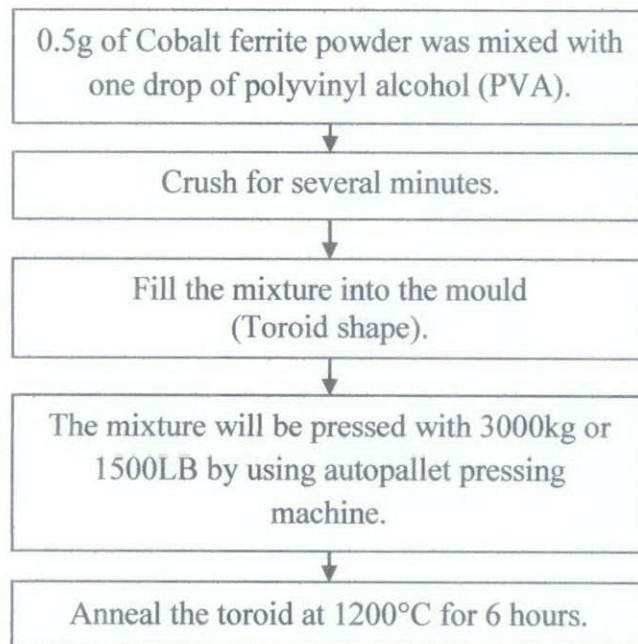


Figure 34: Procedure of making cobalt ferrite in toroid shape.



Figure 35: Carver Press Number 3887 Autopallet press machine.

Table 7: Properties of cobalt ferrite in toroid shape.

Sample	600° C	800° C
Weight (g)	0.5	0.5
Outer Diameter (cm)	0.5	0.5
Inner Diameter (cm)	0.25	0.25
Height (cm)	0.25	0.25
Density (g/cm³)	3.3	3.3
Number of winding	20	20
Material of winding	Copper wire	Copper wire

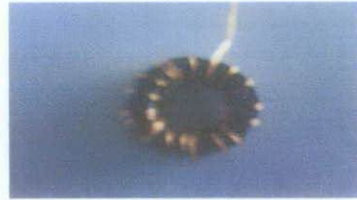


Figure 36: Cobalt ferrite in toroid shape with 20 turns winding.

Initial permeability, Q- factor and relative loss factor (RLF) of the toroids were analyzed by using LCR vector network analyzer. Then, values of L_s and Q factor are calculated. Initial permeability can be calculated by using following formula:

$$\mu_i = \frac{2\pi L_s}{N^2 \mu_o t \ln(D_o / D_i)} \quad (7)$$

Where:

L_s = is the series inductance,

μ_o = is the magnetic permeability,

D_o = is the outer diameter of the toroid,

D_i = is the inner diameter of the toroid, π

N = is the no of turns,

t = is the thickness of the toroid.

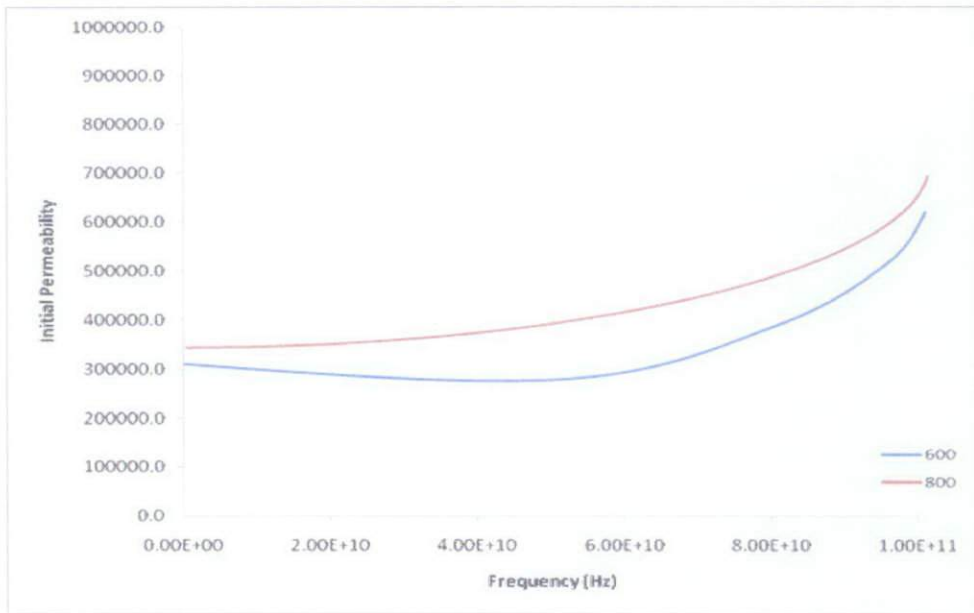


Figure 37: Initial permeability versus frequency for cobalt ferrite toroid.

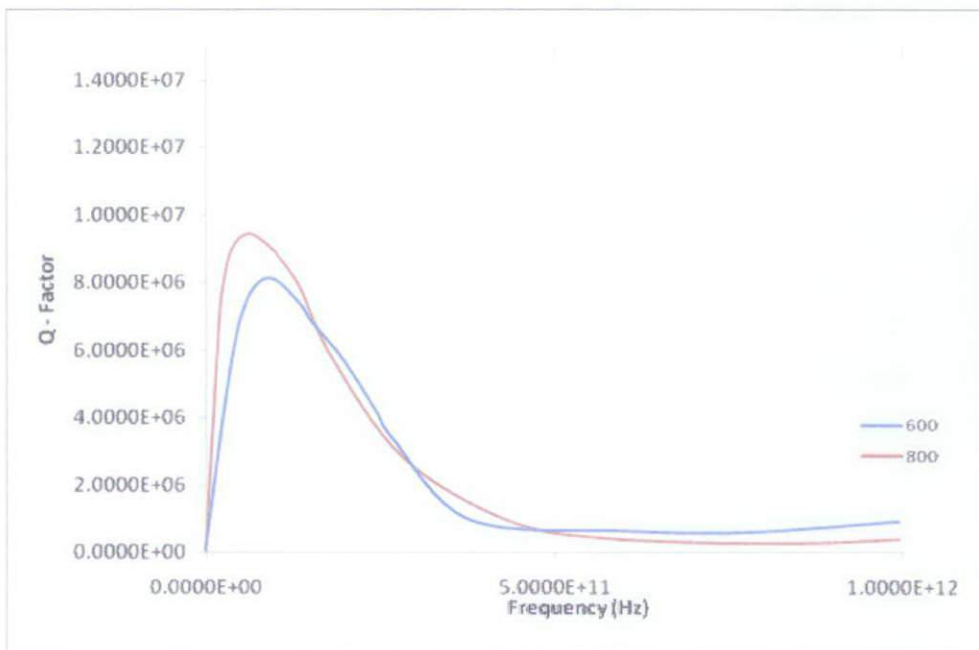


Figure 38: Q-factor versus frequency for cobalt ferrite toroid.

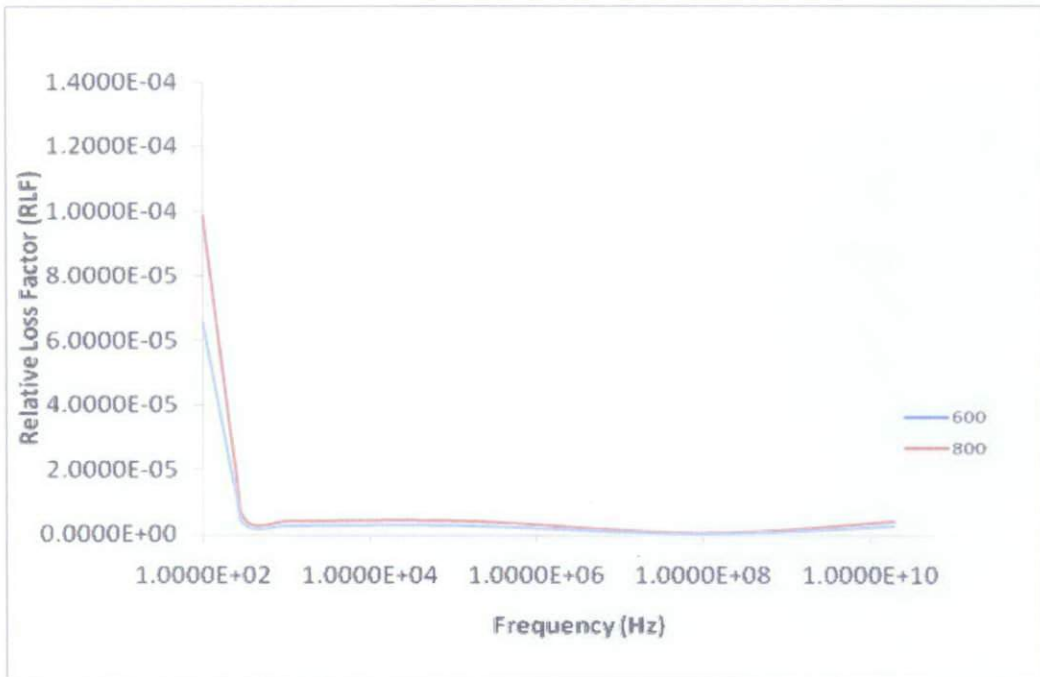


Figure 39: Relative loss factor (RLF) versus frequency for cobalt ferrite

Relative loss factor can be calculated by using following formula:

$$\text{Relative loss factor (RLF)} = \frac{1}{\mu_i Q} \quad (8)$$

Where:

μ_i = is the initial permeability

Q = Q factor [33]

Discussions:

Permeability here means the degree of magnetization of material to response to a magnetic field or the ability of the material to support the formation of magnetic field within itself. From figure 37 the permeability increases when frequency increasing. While, relative loss factor (RLF) decreases as the frequency increases. The grain size would affect directly on the magnetic properties of the soft ferrites. All ferrites have higher relative loss factor (RLF) at lower frequencies (kHz) range, which may be due to higher hysteresis loss arising from their porous structures. The result also shows that the Q-factor increases when frequency increasing and start to decrease at one point. The Q-factor depends on the microstructure of the ferrites for example pores, grain size, and second phase.

Conclusions:

For this project, cobalt ferrite powder annealed at temperature 800°C is chosen to be nanofluid that will be injected inside reservoir model. From XRD result, the crystallite size of the cobalt ferrite powder annealed at 800°C is 5.1171nm, calculated by using Scherer's equation. While, FESEM result shows the grain size is in range 26nm-36nm. The initial permeability of cobalt ferrite powder was found to increase and relative loss factor decreased at high frequency. Hence, cobalt ferrite prepared at 800°C exhibit good crystal structure, fine grain size, and good magnetic properties. Cobalt ferrite nanofluid was prepared by dispersing 5g cobalt ferrite nanopowder and 5g Sodium Dodecyl Sulphate (SDS) in 500ml deionized water and ultrasonicated for 2 hours, which then injected into a packed glass bead pack (reservoir model).

4.3 Transmitter design and analysis

4.3.1 Material selection of antenna

Different materials were investigated to obtain the characteristic information such as permeability, permittivity, conductivity, and resistivity. These potential materials would be used to construct the antenna for this project. The findings are tabulated in the Table 10.

Table 8: Conductivity of some common materials at 20°C [34]

MATERIAL	CONDUCTIVITY, σ (S/m)
Silver	6.2×10^7
Copper	5.8×10^7
Gold	4.1×10^7
Aluminium	3.5×10^7
Iron	10^7
Mercury	10^6
Carbon	3×10^4

There are three main electromagnetic constitutive parameters of a material medium. They are; electrical permittivity ϵ , magnetic permeability μ , and conductivity σ . The conductivity of a material is a measure of how easily electrons can travel through the material under the influence of an external electric field. Based on the Table 10, silver shows the highest value of conductivity followed by copper and aluminium. Even though it has higher conductivity, it is still quite expensive as compared to the copper and aluminium. Therefore in our application we will consider only these two materials which are easily available in the lab which is aluminium.

4.3.2 *Experiment 1: The effect of shape of transmitter and the position of receiver.*

This experiment was conducted in order to understand that results of detector to receive frequency from the curve shape would be exceeding the straight shape transmitter. Ferrite bar with 80 turns winding was used as detector which is connected to the oscilloscope. Besides that, the effect of different placement or position of the detector is observed.

An Agilent 33250A 80MHz Function Generator is used to generates frequency up to 80MHz to the transmitter.

Table 9: Set up of straight shape transmitter

Specification	Details
Type of material	Aluminium rod
Shape	Straight
Diameter of rod (m)	0.009
Length(m)	0.3
Distance between transmitter and detector(m)	0.11

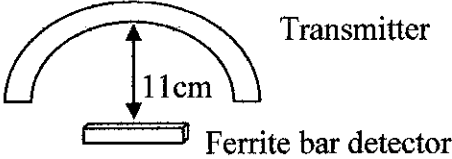
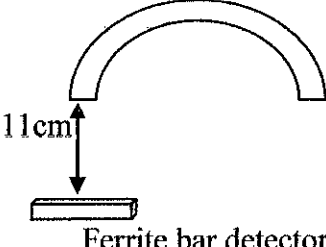
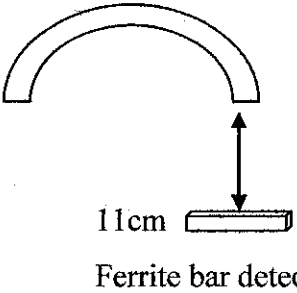
Table 10: Set up of curve shape transmitter

Specification	Details
Type of material	Aluminium rod
Shape	Semi circle
Diameter of rod (m)	0.009
Length(m)	0.3
Diameter of transmitter(m)	0.19
Distance between transmitter and detector(m)	0.11

Table 11: Straight aluminium transmitter voltage and frequency profile.

Condition 1			
Vi(V)	F (MHz)	V _{opp ave} (mV)	f _{ave} (MHz)
10	20	73.20	25.43
10	40	72.48	50.02
10	60	105.10	94.55
10	80	46.03	220.64
Condition 2			
Vi(V)	F (MHz)	V _{opp ave} (mV)	f _{ave} (MHz)
10	20	68.67	23.44
10	40	66.45	40.78
10	60	104.00	70.45
10	80	37.32	209.92
Condition 3			
Vi(V)	F (MHz)	V _{opp ave} (mV)	f _{ave} (MHz)
10	20	78.65	21.34
10	40	75.86	41.12
10	60	112.77	70.53
10	80	40.80	232.16

Table 12: Semi-circle aluminium transmitter voltage and frequency profile.

Condition 1			
			
Vi(V)	F (MHz)	V _{opp ave} (mV)	f _{ave} (MHz)
10	20	128.70	28.46
10	40	141.60	48.02
10	60	164.56	64.70
10	80	80.87	611.34
Condition 2			
			
Vi(V)	F (MHz)	V _{opp ave} (mV)	f _{ave} (MHz)
10	20	108.56	411.44
10	40	129.44	65.93
10	60	123.65	61.12
10	80	70.45	456.11
Condition 3			
			

V_i (V)	F (MHz)	$V_{opp\ ave}$ (mV)	f_{ave} (MHz)
10	20	106.33	539.34
10	40	120.45	70.92
10	60	133.44	58.53
10	80	72.10	441.03

Discussion:

The experiment was conducted to compare the efficiency between a straight and semi circle aluminium rod transmitter. The input peak to peak voltage, V_{ipp} was maintained at 10V $_{ipp}$ and the electromagnetic frequency was vary to observe its effect on the output of two consecutive peak voltage, V_{opp} and the average output frequency, f_{ave} .

The result shows that by using semi circle, transmitter detector was receiving high output frequency compare to straight transmitter. By focusing at condition 1, it can conclude that at this position, high voltage and high frequency is receive. Therefore, condition 1 is selected as the best position for the main experiment oil recovery.

4.4 Oil recovery

4.4.1 Experiment 1: Porosity and Permeability Test for Glass Beads Mixture.

This experiment was conducted in order to evaluate the glass beads mixture characteristics which are the porosity, pore volume and permeability. The glass beads size that available in the lab are (30 – 60) μm , (90 – 150) μm , and (425 – 600) μm . Firstly, the glass beads have been mixed to 3 samples as below:

Table 13: Glass Beads Mixture

Sample	Glass beads mixture
A	150g (30 – 60) μm and 150g (90 – 150) μm
B	150g (90 – 150) μm and 150g (425 – 600) μm
C	150g (30 – 60) μm and 150g (425 – 600) μm

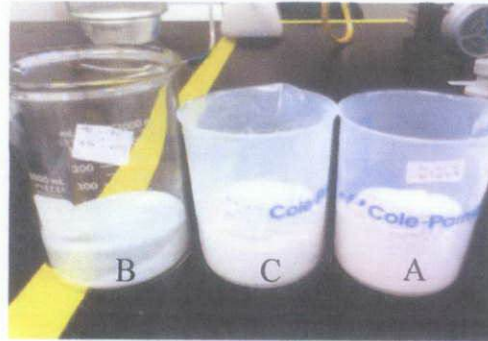


Figure 40: Glass beads mixture

The purpose of using different mixture size of glass beads is to get different pore sizes. Then, the glass beads samples will be packed into the cylindrical PVC column. The weight of cylindrical PVC column with glass beads is recorded for each sample A, B and C.

The permeability of the glass beads pack is a measure of the ease with which the glass beads pack will permit the passage of brine. Next step, the cylindrical PVC column was set up as Figure 41, where a JASCO PU-2080 Plus pump is used to flow the brine through the pressure gauge and cylindrical PVC column at constant flow rate, 2ml/min. Then, the pressure is measured for every 10 minutes and the experiment will be stopped until reach the constant pressure. Here, the area and the length of the cylindrical PVC column are known. Darcy's formula can be expressed as [35]:

$$k = \frac{Q\mu L}{A\Delta P} \quad (9)$$

Where;

k = the permeability of the sample (mD)

Q = the flow rate (ml/s)

μ = the viscosity of the fluid (cp)

L = the length of the cylindrical PVC column (cm)

A = the area of the cylindrical PVC column (cm²)

ΔP = Pressure (atm)

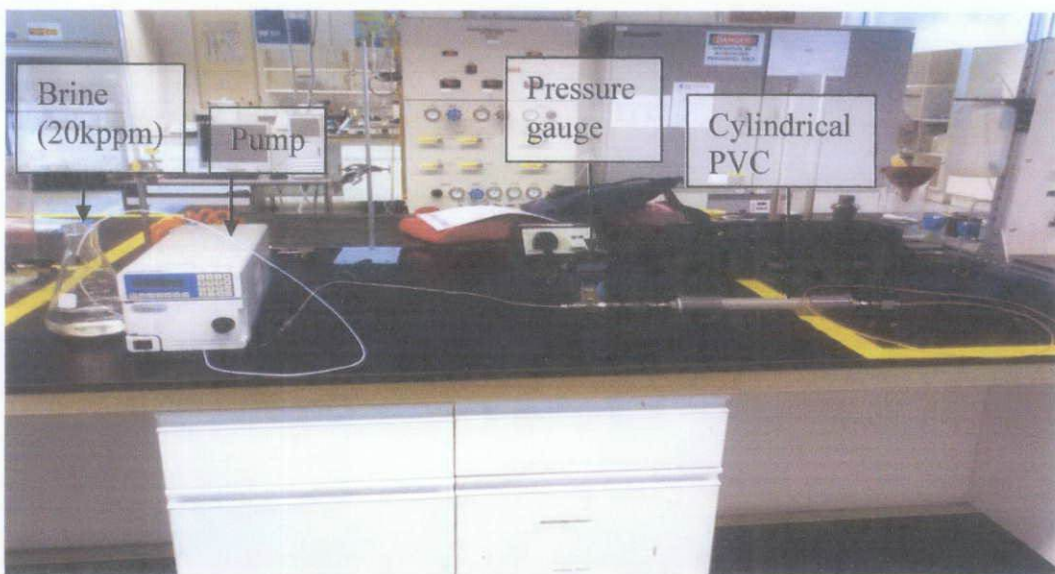


Figure 41: Experiment setup

After that, the wet weight of the glass beads pack is recorded. Porosity of the glass beads pack is defined by the ratio [36]:

$$\phi = \frac{V_V}{V_T} \quad (10)$$

Where;

ϕ = Porosity ratio

V_V = Volume of void-space (such as fluids) (cm³)

V_T = Bulk Volume (cm³)

Table 14: Measurement for permeability test

Sample	A	B	C
Flow rate, Q (ml/s)	0.0333	0.0333	0.0333
Viscosity of brine, μ (cp) (at room temperature)	1.02	1.02	1.02
Length of PVC column, L(cm)	22	22	22
Area of PVC column, A (cm ²)	7.0686	7.0686	7.0686
Pressure, ΔP (atm)	0.1973	0.0204	0.0272
Permeability, k (mD)	535.81	5182.07	3886.55

Table 15: Measurement for porosity test

Sample	A	B	C
Dry weight (PVC + glass beads) (g)	487.98	496.03	516.06
Wet weight (PVC + glass beads + brine) (g)	536.74	552.52	566.87
Pore mass @ brine mass (wet weight – dry weight) (g)	43.76	56.49	50.81
Brine density (20kppm at room temperature) (g/cm ³)	1.0106	1.0106	1.0106
Pore volume, V_v (Brine mass/brine density) (cm ³)	43.30	55.90	50.28
Bulk volume, V_T (L x A) (cm ³)	155.5092	155.5092	155.5092
Porosity (%)	27.84	35.95	32.33

Discussions:

The permeability and the porosity of glass beads sample A is the lowest compare to sample B and C. It is clear that permeability will depend on porosity, the lower porosity the lower the permeability. The smaller the grains, the smaller pores and pore throats, the lower permeability. Besides that, the smaller grain size, the larger the exposed surface area to the flowing fluid, which leads to larger friction between the fluid and the rock, and hence lower permeability.

Conclusion:

For this project, glass beads sample A is chosen to be reservoir model or core rock model. This is because glass beads sample A has the lowest porosity and permeability which we assume as the harder the brine and oil to flow through the glass beads sample. As we know, crude oil is difficult to recover from the reservoir.

4.4.2 Experiment Setup

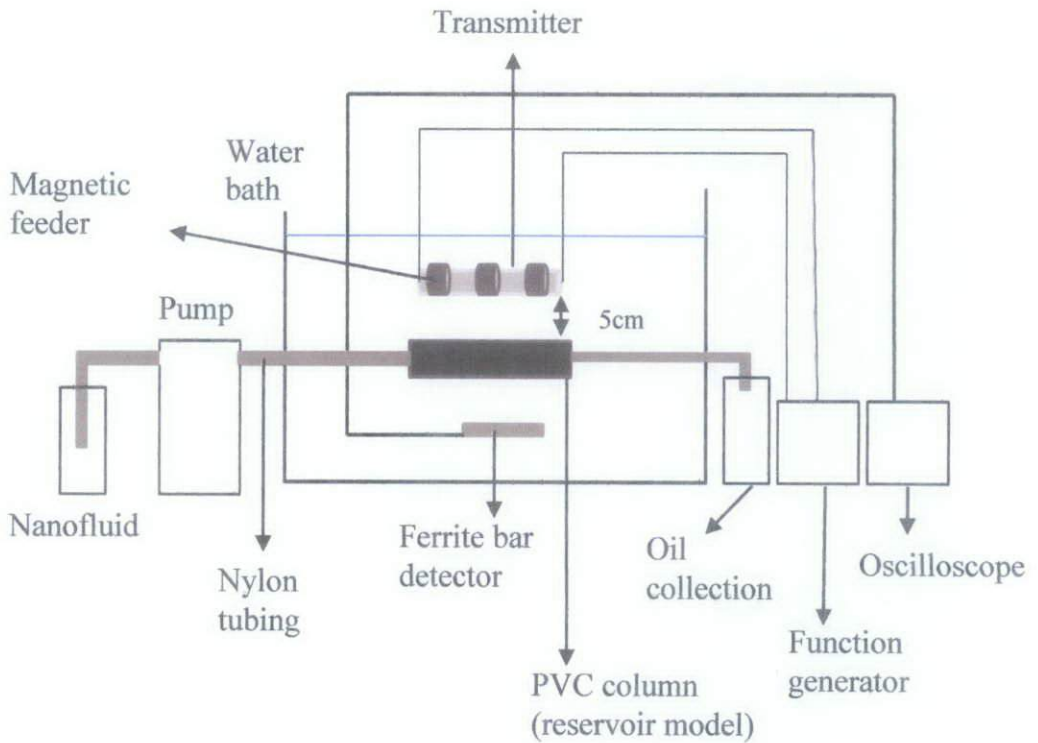


Figure 42: Schematic diagram experiment setup

Figure above shows the basic set up of the experiment that been conduct in the lab. The 1 KHz function generator is used to supply AC current for the transmitter. Magnetic feeder is used to amplify the transmitted waves. A conductive environment was created by filling the aquarium with the salt water which has density $1.0106\text{g}/\text{cm}^3$. The distance transmitter to the PVC column is fixed. The experiment is conducted with injection nanofluid and the glass beads sample in the PVC column is exposed to the EM waves for 24 hours. Finally the percentage of oil recovery is calculated. Figure below shows the real experiment setup that been conducted in the lab.

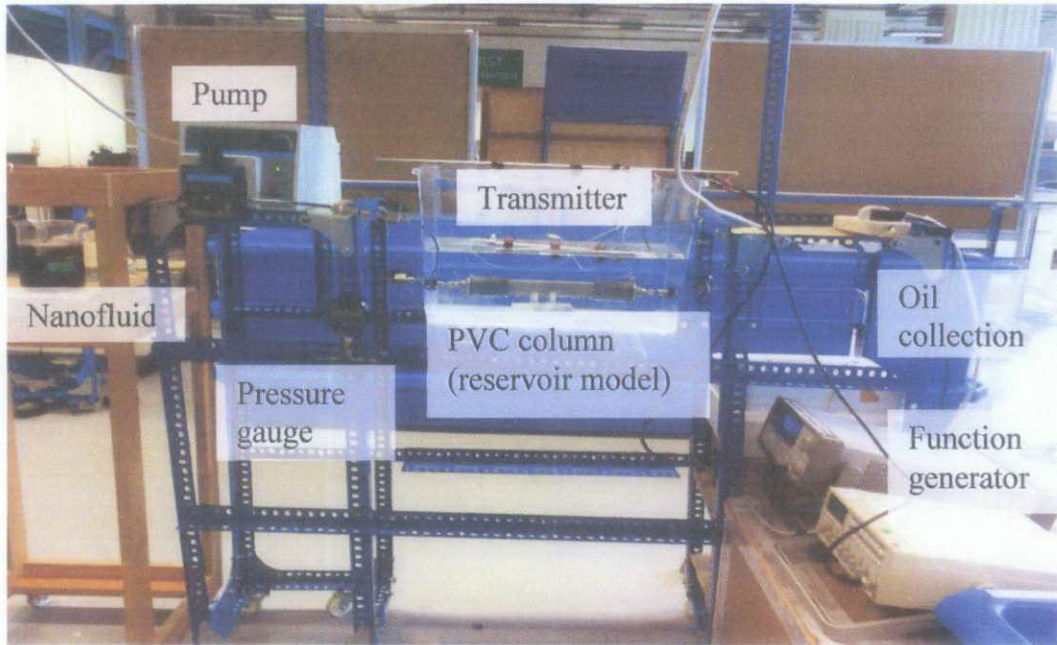


Figure 43: Experiment setup

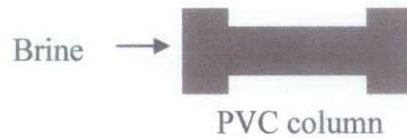
4.4.3 Experiment 2: Oil recovery by using nanofluid injection

Objective: To evaluate the percentage oil recovery from glass beads pack without electromagnetic wave transmission.

Below is the step and details of the experiment:

Step 1:

Objective: To calculate pore volume.



Saturate the glass beads pack with brine until constant pressure is achieved.

The value of flow rate, q ; brine density, μ ; Length, L and area, A of PVC column is fixed.

$$q = 2 \text{ ml/min}$$

$$\mu = 1.02 \text{ cp}$$

$$L = 22 \text{ cm}$$

$$A = 7.0686 \text{ cm}^2$$

Result and Discussion:

- Pore/empty space in the glass beads pack is filled by the brine.
- By using Darcy formula, permeability of the glass beads pack is calculated.

$$\text{Permeability, } k = \frac{Q\mu L}{A\Delta P}$$

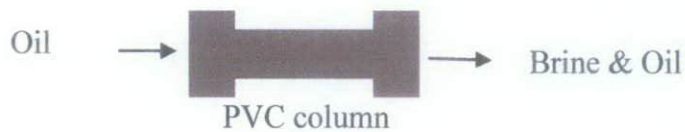
At constant pressure, P 2.8Psi or 0.1973atm, permeability is 535.81mD.

- Pore volume is calculated as follow:

Dry weight (PVC + glass beads) (g)	487.79
Wet weight (PVC + glass beads + brine) (g)	536.40
Pore mass @ brine mass (wet weight – dry weight) (g)	48.61
Brine density (20kppm at room temperature) (g/cm ³)	1.0106
Pore volume, V _v (Brine mass/brine density) (cm ³)	48.10

Step 2:

Objective: To calculate original oil in place (OOIP).



Crude oil injection can be started when stability is reached (constant pressure), until continue oil drop can be seen on the top of the brine collection.

Result and Discussion:

- During oil injection process, brine will be displaced out through a tube and continue oil drop can be seen on the top of the brine collection. This condition show that the glass beads pack saturated with oil.
- The volume of the brine displaced from the glass beads pack will be equal to the volume of the crude oil going into the glass beads pack. This volume represents the amount of original oil in place (OOIP).

$$\begin{aligned} \text{OOIP} &= \text{volume of water displaced (assume } 1 \text{ cm}^3 = 1 \text{ ml)} \\ &= 46.0 \text{ ml} \end{aligned}$$

Volume of water displaced = Volume of oil injected into the glass beads pack.

$$\begin{aligned} \% \text{ OOIP} &= \frac{\text{Volume of water displaced}}{\text{Pore volume}} \times 100\% \\ &= \frac{46.0}{48.10} \times 100\% \\ &= 95.63\% \end{aligned}$$

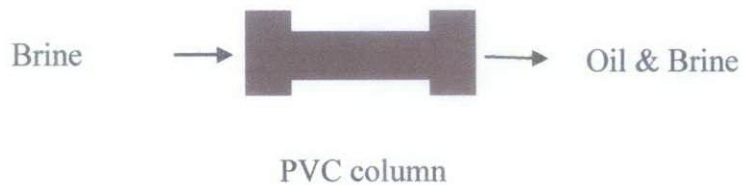
As a conclusion, 95.63% of brine was displaced by crude oil and 4.37% brine remained in the glass beads pack.



Figure 44: Brine collection for experiment 2

Step 3:

Objective: To imitate water flooding phenomena (secondary recovery stage) and calculate residual oil in place (ROIP)



Brine is injected for second time until when it is confirmed that no more oil drop from the outlet tube after 24 hours.

Result and Discussion:

- Some amount of the crude oil is displaced by the brine. The volume of oil displaced from the glass beads pack represent the volume of oil recovered from the secondary recovery.

Volume of oil from secondary recovery = 34.5ml (assume 1cm³ = 1ml)

For secondary recovery stage:

$$\begin{aligned} \% \text{ Recovery Factor (RF)} &= \frac{\text{Volume of oil from secondary recovery}}{\text{OOIP}} \times 100\% \\ &= \frac{34.5\text{ml}}{46.0\text{ml}} \times 100\% \\ &= 75.0\% \end{aligned}$$

$$\begin{aligned} \text{Residual oil in place (ROIP)} &= \text{OOIP} - \text{Volume of oil from} \\ &\quad \text{secondary recovery} \\ &= 46.0\text{ml} - 34.5\text{ml} \\ &= 11.5\text{ml} \end{aligned}$$

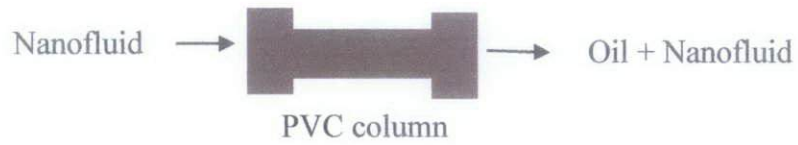
As a conclusion, 11.5ml crude oil or 25% of OOIP remain in the glass beads pack to be recovered in the next recovery stage (EOR).



Figure 45: Oil collection for experiment 2

Step 4:

Objective: To calculate the recovery factor at tertiary recovery stage or EOR.



Nanofluid is injected into the glass beads pack. Experiment is stopped when it is confirmed that no more oil drop from the outlet tube after 24 hours.

Result and Discussion:

- Volume oil recovered from tertiary recovered = 1.0ml (assume 1cm³ = 1ml)

For EOR stage:

$$\begin{aligned} \% \text{ Recovery Factor (RF)} &= \frac{\text{Volume of oil from tertiary recovery}}{\text{ROIP}} \times 100\% \\ &= \frac{1.0}{11.5} \times 100\% \\ &= 8.70\% \end{aligned}$$

As a conclusion, 1.0ml or 8.70% of oil is recovered from 11.5ml ROIP.



Figure 46: Oil recovered without EM wave transmission.

Discussion:

From the experiment, by only injection nanofluid without EM wave transmission to the glass beads pack, the oil recovered is 1.0ml from 11.5ml the remaining oil of the glass beads pack. The percentage of oil recovered is 8.70%.

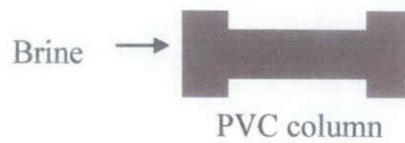
4.4.4 Experiment 3: Oil recovery by using electromagnetic wave transmission and injection nanofluid.

Objective: To evaluate the percentage oil recovery from glass beads pack with electromagnetic wave transmission.

Below is the step and details of the experiment:

Step 1:

Objective: To calculate pore volume.



Saturate the glass beads pack with brine until constant pressure is achieved.

The value of flow rate, q ; brine density, μ ; Length, L and area, A of PVC column is fixed.

$$q = 2 \text{ ml/min}$$

$$\mu = 1.02 \text{ cp}$$

$$L = 22 \text{ cm}$$

$$A = 7.0686 \text{ cm}^2$$

Result and Discussion:

- Pore/empty space in the glass beads pack is filled by the brine.
- By using Darcy formula, permeability of the glass beads sample is calculated.

$$\text{Permeability, } k = \frac{Q\mu L}{A\Delta P}$$

At constant pressure, P 2.8Psi or 0.1973atm, permeability is 535.81mD.

- Pore volume is calculated as follow:

Dry weight (PVC + glass beads) (g)	487.79
Wet weight (PVC + glass beads + brine) (g)	535.35
Pore mass @ brine mass (wet weight – dry weight) (g)	45.56
Brine density (20kppm at room temperature) (g/cm ³)	1.0106
Pore volume, Vv (Brine mass/brine density) (cm ³)	45.08

Step 2:

Objective: To calculate original oil in place (OOIP).



Crude oil injection can be started when stability is reached (constant pressure), until continue oil drop can be seen on the top of the brine collection.

Result and Discussion:

- During oil injection process, brine will be displaced out through a tube and continue oil drop can be seen on the top of the brine collection. This condition show that the glass beads pack saturated with oil.
- The volume of the brine displaced from the glass beads pack will be equal to the volume of the crude oil going into the glass beads pack. This volume represents the amount of original oil in place (OOIP).

$$\begin{aligned} \text{OOIP} &= \text{volume of water displaced (assume } 1\text{ cm}^3 = 1\text{ ml)} \\ &= 42.5\text{ ml} \end{aligned}$$

Volume of water displaced = Volume of oil injected into the glass beads pack.

$$\begin{aligned} \% \text{ OOIP} &= \frac{\text{Volume of water displaced}}{\text{Pore volume}} \times 100\% \\ &= \frac{42.5}{45.08} \times 100\% \\ &= 94.28\% \end{aligned}$$

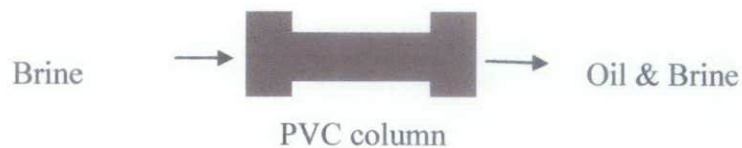
As a conclusion, 94.28% of brine was displaced by crude oil and 5.72% brine remained in the glass beads pack.



Figure 47: Brine collection for experiment 3

Step 3:

Objective: To imitate water flooding phenomena (secondary recovery stage) and calculate residual oil in place (ROIP)



Brine is injected for second time until when it is confirmed that no more oil drop from the outlet tube after 24 hours.

Result and Discussion:

- Some amount of the crude oil is displaced by the brine. The volume of oil displaced from the glass beads pack represent the volume of oil recovered from the secondary recovery.

Volume of oil from secondary recovery = 33.0ml (assume 1 cm³ = 1ml)

For secondary recovery stage:

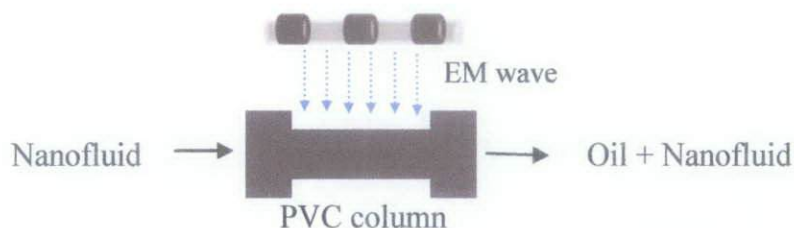
$$\begin{aligned}\% \text{ Recovery Factor (RF)} &= \frac{\text{Volume of oil from secondary recovery}}{\text{OOIP}} \times 100\% \\ &= \frac{33.0\text{ml}}{42.5\text{ml}} \times 100\% \\ &= 77.65\%\end{aligned}$$

$$\begin{aligned}\text{Residual oil in place (ROIP)} &= \text{OOIP} - \text{Volume of oil from} \\ &\quad \text{secondary recovery} \\ &= 42.5\text{ml} - 33.0\text{ml} \\ &= 9.5\text{ml}\end{aligned}$$

As a conclusion, 9.5ml crude oil or 22.35% of OOIP remain in the glass beads sample to be recovered in the next recovery stage (EOR).

Step 4:

Objective: To calculate the recovery factor at tertiary recovery stage or EOR.



Nanofluid is injected into the glass beads sample. A transmitter (1KHz) is placed at 5cm above the PVC column. Experiment is stopped when it is confirmed that no more oil drop from the outlet tube after 24 hours.

Result and Discussion:

- Volume oil recovered from tertiary recovered = 3.0ml (assume $1\text{ cm}^3 = 1\text{ ml}$)

For EOR stage:

$$\begin{aligned}\% \text{ Recovery Factor (RF)} &= \frac{\text{Volume of oil from tertiary recovery}}{\text{ROIP}} \times 100\% \\ &= \frac{3.0}{9.5} \times 100\% \\ &= 31.58\%\end{aligned}$$

As a conclusion 3.0ml or 31.58% of oil is recovered from 9.5ml ROIP.



Figure 48: Oil recovered by using EM wave transmission and injection nanofluid

Discussion:

In this experiment, EM transmitter (1 KHz) was used together with injection nanofluid into the glass beads pack. By using this method, 3.0ml or 31.58% of oil is recovered from 9.5ml ROIP.

Conclusion:

Experiment 2: Oil recovery by using nanofluid injection

Objective: To evaluate the percentage oil recovery from glass beads pack without electromagnetic wave transmission.

Table 16: Calculation of percentage oil recovery for experiment 2

Step	Objective and description	Calculation	Result
1	<p>Objective: To calculate permeability and pore volume.</p> <p>Description: The glass beads pack was saturated with brine until constant pressure is achieved.</p>	<p>Permeability, $k = \frac{Q\mu L}{A\Delta P}$</p> <p>Where;</p> <p>$k$ = the permeability of the sample (mD) Q = the flow rate (ml/s) μ = the viscosity of the fluid (cp) L = the length of the cylindrical PVC column (cm) A = the area of the cylindrical PVC column (cm²) ΔP = Pressure (atm).</p>	<p>At constant pressure, P, 2.8Psi or 0.1973atm, permeability is 535.81mD</p>
		Dry weight = (PVC + glass beads)(g)	487.79g
		Wet weight =(PVC + glass beads + brine) (g)	536.40g
		Pore mass@brine mass = (wet weight – dry weight) (g)	48.61g
		Brine density (20kppm at room temperature) (g/cm ³)	1.0106 g/cm ³
		Pore volume, Vv = (Brine mass/brine density) (cm ³)	48.10 cm ³

2	<p>Objective: To calculate original oil in place (OOIP).</p> <p>Description: Oil is injected until continue oil drop can be seen on the top of the brine collection.</p>	OOIP = volume of water displaced = volume of oil injected into the glass beads pack (assume $1\text{cm}^3 = 1\text{ml}$)	46.0ml
		% OOIP = (Volume of water displaced / pore volume) x 100%	95.63%
3	<p>Objective: To imitate water flooding phenomena (secondary recovery stage) and calculate residual oil in place (ROIP).</p> <p>Description: Brine is injected for second time until when it is confirmed that no more oil drop from the outlet tube after 24 hours.</p>	Volume of oil from secondary recovery	34.5ml
		For secondary recovery stage: % Recovery Factor (RF) = (Volume of oil from secondary recovery / OOIP) x 100%	75.0%
		Residual oil in place (ROIP) = OOIP – Volume of oil from secondary recovery	11.5ml
4	<p>Objective: To calculate the recovery factor at tertiary recovery stage or EOR.</p> <p>Description: Nanofluid is injected into the glass beads pack. Experiment is stopped when it is confirmed that no more oil drop from the outlet tube after 24 hours.</p>	Volume oil recovered from tertiary recovered (assume $1\text{cm}^3 = 1\text{ml}$)	1.0ml
		For EOR stage: % Recovery Factor (RF) = (Volume of oil from tertiary recovery / ROIP) x 100%	8.70%

Experiment 3: Oil recovery by using electromagnetic wave transmission and injection nanofluid.

Objective: To evaluate the percentage oil recovery from glass beads pack with electromagnetic wave transmission.

Table 17: Calculation of percentage oil recovery for experiment 3

Step	Objective and description	Calculation	Result
1	<p>Objective: To calculate permeability and pore volume.</p> <p>Description: The glass beads pack was saturated with brine until constant pressure is achieved.</p>	<p>Permeability, $k = \frac{Q\mu L}{A\Delta P}$</p> <p>Where;</p> <p>$k$ = the permeability of the sample (mD)</p> <p>Q = the flow rate (ml/s)</p> <p>μ = the viscosity of the fluid (cp)</p> <p>L = the length of the cylindrical PVC column (cm)</p> <p>A = the area of the cylindrical PVC column (cm²)</p> <p>ΔP = Pressure (atm)</p>	At constant pressure, P, 2.8Psi or 0.1973atm, permeability is 535.81mD
		Dry weight = (PVC + glass beads) (g)	487.79g
		Wet weight =(PVC + glass beads + brine) (g)	535.35g
		Pore mass@brine mass = (wet weight – dry weight) (g)	45.56g
		Brine density (20kppm at room temperature) (g/cm ³)	1.0106 g/cm ³
		Pore volume, $V_v =$ (Brine mass/brine density) (cm ³)	45.08 cm ³
		2	<p>Objective: To calculate original oil in place (OOIP).</p> <p>Description: Oil is</p>

	injected until continue oil drop can be seen on the top of the brine collection.	$\% \text{ OOIP} = (\text{Volume of water displaced} / \text{pore volume}) \times 100\%$	94.28%
3	Objective: To imitate water flooding phenomena (secondary recovery stage) and calculate residual oil in place (ROIP). Description: Brine is injected for second time until when it is confirmed that no more oil drop from the outlet tube after 24 hours.	Volume of oil from secondary recovery	33.0ml
		For secondary recovery stage: $\% \text{ Recovery Factor (RF)} = (\text{Volume of oil from secondary recovery} / \text{OOIP}) \times 100\%$	77.65%
		Residual oil in place (ROIP) = OOIP – Volume of oil from secondary recovery	9.5ml
4	Objective: To calculate the recovery factor at tertiary recovery stage or EOR. Description: Nanofluid is injected into the glass beads pack. A transmitter (1KHz) is placed at 5cm above the PVC column. Experiment is stopped when it is confirmed that no more oil drop from the outlet tube after 24 hours.	Volume oil recovered from tertiary recovered (assume $1\text{cm}^3 = 1\text{ml}$)	3.0ml
		For EOR stage: $\% \text{ Recovery Factor (RF)} = (\text{Volume of oil from tertiary recovery} / \text{ROIP}) \times 100\%$	31.58%

From experiment 2, the percentage of oil recovered is 8.70% while from experiment 3, the percentage of oil recovered is 31.58%. The percentage of oil recovered from experiment 3 is higher than experiment 2 which is 22.88% improved. This is because, experiment 3 is using electromagnetic wave transmission which helps the ion of the nanofluid to vibrate and the recovery of the remaining oil is caused by the disturbance on the oil-water interfaces that exist due to the creation of elastic waves as the oscillating EM wave imparted on

the pore surfaces. We can say that interfacial tension at oil-water interfaces has been lowered due to the presence of surfactant or nanoparticles. So, reducing surface tension can help the oil easy to flow.

As a conclusion, development magnetic nanoparticles, cobalt ferrite which are used as the medium to absorb EM waves and to reduce interfacial tension between oil-water interfaces to make the oil easily to flow and to control mobility of the reservoir fluids had been proved and at the same time assist the oil recovery from the glass beads pack.

CHAPTER 5

CONCLUSION AND RECOMMENDATION

5.1 Conclusion

This project deals with synthesis of cobalt ferrite nanoparticles via sol-gel method. Cobalt ferrite nanoparticles have been characterized by using X-Ray Diffractions (XRD), Field Emission Scanning Electron Microscope (FESEM) and Energy Dispersive X-Ray (EDX). Based on XRD result, cobalt ferrite powder which annealed with 800°C gives smaller crystallite size and higher intensity which are 5.1171nm and 62 respectively. The morphology of cobalt ferrite, CoFe_2O_4 (particles size) was observed by a FESEM and the particle size for cobalt ferrite for annealed with 800°C gives the smaller size which in the range of 26nm to 36nm. Atomic and weight percentage of cobalt ferrite at 800°C also gives the lowest standard deviation value for all elements. The initial permeability of cobalt ferrite powder was found to increase and relative loss factor decreased at high frequency. Hence, cobalt ferrite prepared at 800°C exhibit good crystal structure, fine grain size, and good magnetic properties.

In this project, we use a straight dipole transmitter due to the strength in lower frequency. Through this project, we had recovered 31.58% of ROIP by supply 1 KHz electromagnetic wave transmission with nanofluid injection compared to only 8.70% of oil recovered by using only nanofluid injection. It is proven that magnetic nanoparticle, cobalt ferrite can be the medium to absorb EM waves and also assist to oil recovery at the same time. Hence, magnetic nanoparticles can be one of the alternatives to improve the crude oil production.

5.1 Recommendation

Several recommendations were made to improve the experiment for future research work.

1. Simulation using CST software of the EM transmitter.
2. The distance between the transmitter's sources can be varied in order to optimize the construction electromagnetic waves production.
3. The frequency sources to the transmitter can be varied and the shape of the transmitter also can be varied instead of using straight transmitter.
4. Change the synthesis method from sol –gel method to self combustion.
5. Instead of using cobalt ferrite, for next experiment we can use cobalt zinc ferrite.
6. Use better solution to make sure the nanoparticle can suspend longer in the fluid. Instead of using Sodium Dodecyl Sulphate (SDS) solution, we also can disperse nanosized powder in aqueous ethylene glycol.

REFERENCES

- [1] Waterfront Technology Solution, Retrieved from http://en.wikipedia.org/wiki/Wavefront_Technology_Solutions, August, (2010).
- [2] Das S., Electro-Magnetic heating in Viscous Oil Reservoir, SPE/PS/CHOA 117693 SPE International Thermal Operations and Heavy Oil Symposium, (2008).
- [3] http://www.rigzone.com/training/insight.asp?insight_id=313&c_id=
- [4] Vermeulen F., In Situ Electromagnetic Heating for Hydrocarbon Recovery and Environmental Remediation, Journal of Canadian Petroleum Technology, , Vol.39, No. 8, (2000).
- [5] Magnetic Nanoparticles, retrieved from http://en.wikipedia.org/wiki/Magnetic_nanoparticles, 29 April, (2011).
- [6] Patil V.G. et al., Journal of Alloys and Compounds 488, 199-203, (2009).
- [7] Dooley J.W., Magnetic Polarization, Physics Department, Millersville University, from <http://muweb.millersville.edu/~jdooley/macro/derive/elpol/capexp/capexp.htm>
- [8] Sajjia M., et al., Journal of Alloys and Compound 506, 400-406, (2010).
- [9] Advantages of sol-gel technologies for biomedical application, retrieved from <http://spiedl.aip.org/getabs/servlet/GetabsServlet?prog=normal&id=PSISDG003567000001000050000001&idtype=cvips&gifs=yes&ref=no>, July, (2010).
- [10] Nanoparticles, retrieved from <http://www.sciencedaily.com/articles/n/nanoparticle.htm>, January, (2010).
- [11] Chakma A. and Jha K. N, Heavy oil recovery from thin pay zones by electromagnetic heating. SPE Paper 24817. 67th Annual Technical Conference and Exhibition, Washington, DC, October 4–7, (1992).

- [12] Islam M. R., and Chakma A, A new recovery technique for heavy-oil reservoirs with bottomwater. SPE 20258. Product. Eng. May, (1992).
- [13] Ulaby F. T., Electromagnetic for Engineers, Pearson Education International, (2005).
- [14] Fawwaz T.U, Magnetostatics, Electromagnetics for Engineers, Pearson Education International, The University of Michigan, (2005).
- [15] Lehrman R.L, Physics the easy way Barron's Educational Series, pp.313, (1998).
- [16] Magnetic field of current.(n.d), Retrieved from <http://hyperphysics.phy-astr.gsu.edu/HBASE/magnetic/magcur.html>, February 2, (2009).
- [17] Islam M.R., Enhanced Oil Recovery of Ugnu Tar Sands of Alaska Using Electromagnetic Heating with Horizontal Wells, EMERTEC Developments Inc. and S.S Wadader and A.Bansal, U.of Alaska Fairbanks, (1992).
- [18] Magnetic field of current loop.(n.d). Retrieved from <http://hyperphysics.phy-astr.gsu.edu/HBASE/magnetic/curloo.html>, February 2, (2009).
- [19] Maxwell's Equation and Electromagnetic Wave, Retrieved from http://galileoandeinstein.physics.virginia.edu/more_stuff/Maxwell_Eq.html, September, (2009).
- [20] Karl J.E., Jared D.A., David L. W. and Aldo T.M., Numerical Study of Electromagnetic Waves Generated by a Prototype Dielectric Lagging Tool, Geophysics; Vol.69, No.1, pp. 64-77, January-February, (2004).
- [21] Permeability and saturation. (n.d), Retrieved from http://www.allaboutcircuit.com/vol_1/hpt_14/4.html, March 30, (2009).
- [22] Ida N., Engineering electromagnetic. Springer, pp.546-548, (2004).
- [23] Journal of Colloid and Interface Science, Vol.241, 509–513, (2001).
- [24] Interfacial Tension, Retrieved from <http://web.mit.edu/nmf/education/wettability/interfacial.html>, September, (2010).

- [25] Interfacial Tension, Retrieved from <http://www.attension.com/interfacial-tension.aspx>, January, (2011).
- [26] Surface Tension, Retrieved from http://en.wikipedia.org/wiki/Surface_tension, February, (2011).
- [27] Mundimax companies, Magnetizer commercial and industrial Oil Line Energizers, Retrieved from http://www.mundi.com/Mag_Oil_Apps.pdf, March 22, (2010).
- [28] Azároff, L. Kaplow R., Kato N., Weiss R. J., Wilson A. J. C., Young R. A., X-ray diffraction. McGraw-Hill, (1974).
- [29] Fathehah Bt Mohamd Azman, Magnetic Nanoparticles for Enhanced Oil Recovery (EOR) Using EM Methods, BSc. Dissertation, Universiti Teknologi PETRONAS, (2010).
- [30] Field Emission Scanning Electronic Microscopy, Retrieved from <http://www.photometrics.net/fesem.html>, August, (2010).
- [31] X-ray Scattering Techniques, Retrieved from http://en.wikipedia.org/wiki/X-ray_scattering_techniques, July, (2009).
- [32] Klung H. P., Alexander L. E., X-ray diffraction procedure for polycrystalline procedure for polycrystalline and amorphous materials, wiley, New York, (1974).
- [33] Roy P.K., Bera J., Characterization of nanocrystalline NiCuZn ferrite powder synthesized by solgel auto combustion method , J.Mat.Proc.Tech, Vol.197, pp.279-283, (2008).
- [34] Ulaby, F. T. Electromagnetic for Engineers, Pearson Education International, (2005).
- [35] Dr. Paul Glover, Petrophysics MSc Course Notes, PERMEABILITY, pg.21
- [36] Porosity, Retrieved from <http://en.wikipedia.org/wiki/Porosity>, December, (2010).